A root-knot nematode effector Mi2G02 hijacks a host plant trihelix transcription factor for nematode parasitism

Jianlong Zhao, Kaiwei Huang, Rui Liu, Yuqing Lai, Pierre Abad, Bruno Favery, Heng Jian, Jian Ling, Yan Li, Yuhong Yang, et al.

Journal Pre-proof

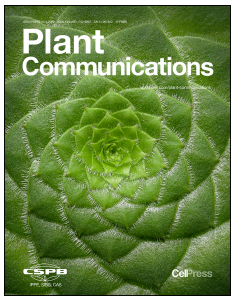

A root-knot nematode effector Mi2G02 hijacks a host plant trihelix transcription factor for nematode parasitism

Jianlong Zhao, Kaiwei Huang, Rui Liu, Yuqing Lai, Pierre Abad, Bruno Favery, Heng Jian, Jian Ling, Yan Li, Yuhong Yang, Bingyan Xie, Michaël Quentin, Zhenchuan Mao

PII: S2590-3462(23)00269-9

DOI: https://doi.org/10.1016/j.xplc.2023.100723

Reference: XPLC 100723

To appear in: *PLANT COMMUNICATIONS*

Received Date: 3 July 2023

Revised Date: 12 August 2023

Accepted Date: 19 September 2023

Please cite this article as: Zhao, J., Huang, K., Liu, R., Lai, Y., Abad, P., Favery, B., Jian, H., Ling, J., Li, Y., Yang, Y., Xie, B., Quentin, M., Mao, Z., A root-knot nematode effector Mi2G02 hijacks a host plant trihelix transcription factor for nematode parasitism, *PLANT COMMUNICATIONS* (2023), doi: https://doi.org/10.1016/j.xplc.2023.100723.

A root-knot nematode effector Mi2G02 hijacks a host plant trihelix transcription factor for nematode parasitism

Jianlong Zhao[1,4,*], Kaiwei Huang[1,4], Rui Liu[1,4], Yuqing Lai[1], Pierre Abad[2], Bruno Favery[2], Heng Jian[3], Jian Ling[1], Yan Li[1], Yuhong Yang[1], Bingyan Xie[1], Michaël Quentin[2,*] and Zhenchuan Mao[1,*]

[1] State Key Laboratory of Vegetable Biobreeding, Institute of Vegetables and Flowers, Chinese Academy of Agricultural Sciences, 100081, Beijing, China

[2] INRAE, Université Côte d'Azur, CNRS, ISA, F-06903, Sophia Antipolis, France

[3] Department of Plant Pathology and Key Laboratory of Pest Monitoring and Green Management of the Ministry of Agriculture, China Agricultural University, 100193, Beijing, China

[4] These authors contributed equally: Jianlong Zhao, Kaiwei Huang, Rui Liu.

*** Corresponding:** Email: Jianlong Zhao (zhaojianlong@caas.cn), Michaël Quentin (michael.quentin@inrae.fr), Zhenchuan Mao (maozhenchuan@caas.cn).

Running title

Mi2G02 effector stabilizes a transcription factor

Short summary

Root-knot nematodes establish parasitic relationships with host plants through secreting effectors. In this study, we highlight the role of Mi2G02 effector and its target GT-3a, a trihelix transcription factor, in plant nucleus. Mi2G02 maintains GT-3a protein stabilization by inhibiting the 26S proteasome-dependent pathway, leading to a suppression of *TOZ* and *RAD23C* expression, promoting *Meloidogyne incognita* parasitism.

ABSTRACT

Root-knot nematodes (RKNs) cause huge agricultural losses every year. They secrete a repertoire of effectors to facilitate parasitism through the induction of plant-derived giant feeding cells, which serve as their sole source of nutrients. However, the mode of action of these effectors and host targeted proteins remain largely unknown. In this study, we investigated the role of the effector Mi2G02 in

Meloidogyne incognita parasitism. Host-derived *Mi2G02* RNA interference in *Arabidopsis thaliana* affects giant cells development, whereas the ectopic expression of Mi2G02 promotes root growth and increases plant susceptibility to *M. incognita*. We used various combinations of approaches to study the specific interactions between Mi2G02 and *A. thaliana* GT-3a, a trihelix transcription factor. *GT-3a* knockout in *A. thaliana* affected feeding site development, resulting in the production of fewer egg masses, whereas *GT-3a* overexpression in *A. thaliana* increased susceptibility to *M. incognita* and also root growth. Moreover, we highlight the role of Mi2G02 in maintaining GT-3a protein stabilization by inhibiting the 26S proteasome-dependent pathway, leading to a suppression of *TOZ* and *RAD23C* expression, promoting nematodes parasitism. Thus, this work enhances our understanding of the manipulation of the role and regulation of a transcription factor by a pathogen effector through interfering proteolysis pathway to reprogram genes expression for nematode feeding cells development.

Keywords: *Meloidogyne incognita*, effector, giant cell, Mi2G02, transcription factor, interaction

INTRODUCTION

Root-knot nematodes (RKNs; *Meloidogyne* spp.) can infect thousands of plant species, causing huge agricultural losses every year (Abad et al., 2008; Jones et al., 2013). RKN juveniles induce the redifferentiation of plant vascular cells to establish feeding structures that support their development into reproductive adult females (Bartlem et al., 2014). The second-stage juveniles (J2s) enter the host in the root elongation area and migrate intercellularly toward the vascular tissues, where they select five to seven parenchyma cells, into which they inject esophageal gland secretions through a syringe-like stylet (Favery et al., 2020). These secretions contain proteinaceous effectors, which reprogram the root cells to become giant cells (GCs), hypertrophied multinucleate feeding cells that undergo several rounds of nuclear division without cell division and extensive endoreduplication, with expansion by isotropic growth (Caillaud et al., 2008). The cells surrounding the GCs simultaneously divide, to form a typical root-knot or gall. The vascular tissues undergo extensive reorganization, and the xylem proliferates (Baldacci-Cresp et al., 2020; Bartlem et al., 2014; Yamaguchi et al., 2017). GCs are the only source of nutrients for RKNs throughout their live cycle; the

nematode must, therefore, maintain this parasitic interaction for several weeks, until the female can lay her eggs in a gelatinous matrix on the outside of the root tissues (Favery et al., 2020).

This intricate biotrophic interaction requires the nematode to cope with host defense responses, to alter host-cell morphology and to hijack the physiology of host cells for its own benefit. The nematode achieves these ends by inducing a deep transcriptional reprogramming of host cells, as demonstrated by a large number of transcriptomic studies (Barcala et al., 2010; Cabrera et al., 2014; Escobar et al., 2011; Fuller et al., 2007; Jammes et al., 2005; Olmo et al., 2017; Portillo et al., 2009; Przybylska and Spychalski, 2021; Sato et al., 2021; Shukla et al., 2018; Warmerdam et al., 2018; Yamaguchi et al., 2017; Zhu et al., 2022). Genes encoding transcription factors (TFs), which regulate key expression by binding to appropriate DNA elements and recruiting additional proteins to initiate transcription (Strader et al., 2022), are among the genes known to display differential expression in galls (Cabrera et al., 2014; Przybylska and Spychalski, 2021; Yamaguchi et al., 2017; Zhu et al., 2022). Many of these plant TFs are known to be key players in the regulation of plant developmental processes and stress responses. They include ETHYLENE-RESPONSIVE FACTORS (ERF), NO APICAL MERISTEM (NAC), AUXIN RESPONSE FACTORS (ARF) and LATERAL ORGAN BOUNDARIES DOMAIN-(LBD) (Shukla et al., 2018). However, very little is known about the role of these TFs in GC formation and RKNs parasitism. For LBD16, inactivation led to a decrease in infection or even a total absence of feeding site formation (Cabrera et al., 2014; Olmo et al., 2017).

RKN effectors are clearly involved in modulating host transcriptional responses. They may act as transcription factors, as has been shown for the *M. incognita* effector 7H08, which localizes to the plant cell nucleus and functions as a transcriptional activator (Zhang et al., 2015). Other effectors may associate with and dysregulate host transcription factors. Mi16D10 may be one such effector, as it has been shown to interact with plant SCARECROW-like transcription factors known to regulate root development (Huang et al., 2006). Another example is provided by MiEFF18, an effector that interacts with the spliceosomal protein SmD1 to trigger alternative splicing events during pre-mRNA maturation in galls, thereby increasing the diversity of host transcripts (Mejias et al., 2021; Mejias et al., 2022).

M. incognita secreted protein 2 (*Mi-msp2 or Mi2G02*) was initially identified as a putative parasitism gene expressed exclusively in the subventral esophageal gland cells of parasitic J2s (Huang et al., 2003). It was subsequently shown to be required for *M. incognita* parasitism in host-derived RNA interference experiments (Joshi et al., 2022; Joshi et al., 2019). *Mj2G02,* an ortholog from *M. javanica*, has been shown to suppress Gpa2/RBP-1-triggered cell death in *Nicotiana benthamiana* and jasmonate-mediated plant immune responses (Song et al., 2021). 2G02 proteins are nuclear effectors; they have a ShK toxin (ShKT) domain encoding a potassium channel inhibitor first identified in a sea anemone (*Stichodactyla helianthus*) (Tudor et al., 1996). Proteins containing ShKT domains are widely expressed in parasitic and non-parasitic nematodes (Hewitson et al., 2013). There is evidence to suggest that ShkT-like domains act as contact surfaces for protein interactions (Thein et al., 2009) and for immune evasion (Chhabra et al., 2014; Niu et al., 2016; Song et al., 2021). However, the plant target proteins by Mi2G02 are unknown.

In this study, we show that the Mi2G02 effector interacts with an *Arabidopsis thaliana* trihelix transcription factor, GT-3a, and that this interaction is important for nematode parasitism. We also demonstrate that GT-3a functions as a transcription inhibitor, binding to the promoters of *TOZ* and *RAD23C*, thereby modulating plant cell development for *M. incognita* parasitism. We found that Mi2G02 stabilized GT-3a by inhibiting the 26S proteasome-dependent pathway, thereby causing a stronger suppression of *TOZ* and *RAD23C* expression. Collectively, these results demonstrate the involvement of a *M. incognita* effector (Mi2G02), a plant transcription factor (GT-3a), and downstream regulatory genes in the formation and development of multinucleate GCs for nematode parasitism.

RESULTS

Mi2G02 is a nematode nuclear effector essential for giant cell development

Mi2G02/MiMSP2 gene encodes a 210-amino acid (aa) protein with an 18 aa N-terminal signal peptide (SP), a ShK toxin (ShKT) domain (33–69 amino acids) and two nuclear localization signals (NLS-1 and NLS-2), one of which is located in the ShKT domain (Figure 1A). Transient expression assays were performed in *Nicotiana benthamiana* leaves, to investigate the functionality of the NLSs *in planta*. Mi2G02-GFP recombinant fusion proteins were detected exclusively in the plant cell nucleus, exclusively in the nucleoplasm, with exclusion from the nucleolus (Figure 1B). We

mutated the two predicted nuclear localization signals in the effector sequence, to generate Mi2G02-mu1 (mutated NLS-1), Mi2G02-mu2 (mutated NLS-2) and Mi2G02-mu3 (mutated NLS-1 and NLS-2) (Figure 1A). Mi2G02-mu1-GFP, Mi2G02-mu2-GFP and Mi2G02-mu3-GFP were found principally in the cytoplasm (Figure 1B). Immunoblotting using cytoplasmic and nuclear fraction proteins extracted from *N. benthamiana* plant leaves confirmed the nuclear expression of Mi2G02-GFP, but not Mi2G02-mu1-GFP, Mi2G02-mu2-GFP and Mi2G02-mu3-GFP (Figure 1C). These results demonstrated the requirement of both NLSs for the localization of Mi2G02 to the nucleus.

We investigated the role of Mi2G02 in giant cell formation, by generating three homozygous RNAi *A. thaliana* lines expressing the *Mi2G02* hairpin dsRNA. The expression of the hairpin construct in these RNAi lines was confirmed by PCR (Supplemental Figure 1A) and the transgenic plants were inoculated with nematodes. The silencing of *Mi2G02* by host-derived RNAi was validated by RT-qPCR in feeding nematodes recovered from the infested plants (Figure 2A and Supplemental Figure 1B). Consistent with previous findings (Joshi et al., 2019), *Mi2G02* silencing decreased the numbers of galls and egg masses by at least 60% in the *Mi2G02* RNAi lines relative to the two control lines: wild-type plants and a *GFP* RNAi line (Figure 2B and Supplemental Figure 1B). We investigated the role of Mi2G02 in the formation of RKN-induced feeding sites further, by analyzing the morphology of the feeding cells induced in the RNAi lines. All three *Mi2G02* RNAi lines showed significantly smaller (30%) GC areas than the controls (Figure 2C). These findings suggest that *Mi2G02* plays a role in nematode parasitism, particularly in the development of GCs.

We then generated two transgenic *A. thaliana* lines with ectopic *Mi2G02* expression. Semiquantitative RT-PCR (Supplemental Figure 2A) and western blot (Supplemental Figure 2B) were performed to confirm the expression of *Mi2G02* in the transgenic plants. Interestingly, the roots of the *Mi2G02*-expressing transgenic lines were 27% and 33% longer (n=10) in the two independent lines than those of the wild-type plants (Figure 2D and Supplemental Figure 3C). In nematode inoculation assays, both transgenic lines were significantly ($P < 0.05$) more susceptible to *M. incognita* infection than wild-type plants; the *Mi2G02*-expressing lines had up to 30% more galls and egg masses than the wild-type plants at 35 dpi (Figure 2E and Supplemental Figure 2D). Mi2G02 is, therefore, an effector essential for *M. incognita* parasitism, and able to modulate root growth.

Mi2G02 interacts with the trihelix transcription factor GT-3a

We used a yeast two-hybrid (Y2H) screen to identify the proteins of *A. thaliana* targeted by Mi2G02. We used a signal peptide-deficient Mi2G02 as a bait to screen a cDNA library from *M. incognita*-infected *A. thaliana* roots. We identified 20 candidate target proteins, including six proteins annotated as predicted nuclear proteins in TAIR (Supplemental Table 1). Based on the number of captures, and predicted subcellular distributions and functions, we selected three candidate targets for further study: a trihelix transcription factor (GT-3a, AT5G01380), the LATERAL ORGAN BOUNDARIES DOMAIN PROTEIN 41 (LBD41, AT3G020550) and UBIQUITIN EXTENSION PROTEIN 1 (UBQ1, AT3G52990). A pairwise Y2H assay was performed to validate the interactions between Mi2G02 and the full-length GT-3a, LBD41 and UBQ1 proteins. GT-3a was the only protein found to interact with Mi2G02 (Figure 3A and 3B). LBD41 displayed strong auto-activation in yeast, and it was not possible to confirm any interaction between Mi2G02 and UBQ1 (Supplemental Figure 3A).

We investigated the possible involvement of the ShKT domain of Mi2G02 and the DNA-binding domain (DB) of GT-3a in the interaction, by generating two truncated versions of Mi2G02 (Mi2G02-ShKT and Mi2G02-ΔShKT) and two truncated versions of GT-3a (GT-3a-DB and GT-3a-ΔDB) (Figure 3A). Subcellular localization results showed that Mi2G02-ShKT-GFP was localized mainly in the cell nucleus (Supplemental Figure 3B). Pairwise Y2H experiments demonstrated that the ShKT domain of Mi2G02 and the DB domain of GT-3a were required for the interaction between these two proteins (Figure 3B). We also investigated the requirement of the NLSs of Mi2G02 for the interaction with GT-3a in yeast. Pairwise Y2H experiments with Mi2G02-mu1, Mi2G02-mu2 and Mi2G02-mu3 showed that both the NLSs of Mi2G02 were required for interaction with GT-3a (Figure 3C).

The co-expression of Mi2G02-GFP and mcherry-GT-3a in *N. benthamiana* leaf cells showed that the effector and its target were colocalized in the nucleoplasm of the plant cells (Figure 3D). We then investigated the interactions between Mi2G02 and GT-3a *in planta,* by performing bimolecular fluorescence complementation (BiFC) assays. The co-expression of Mi2G02 fused to the N-terminal part of YFP (Mi2G02-nEYFP) and GT-3a fused to the C-terminal part of YFP (GT-3a-cEYFP) in *N. benthamiana* epidermal leaf cells resulted in a reconstitution of YFP activity in the plant cell nucleus, whereas no YFP fluorescence was observed if Mi2G02 with mutated NLSs or an empty vector was used (Figure 3E and Supplemental Figure 3C).

A split luciferase complementation assay (LCA) and a co-immunoprecipitation (Co-IP) assay were performed for further verification of the interaction between Mi2G02 and GT-3a *in planta*. A positive luciferase signal was obtained when Mi2G02 was co-expressed with GT-3a in *N. benthamiana* leaves, as luciferase activity was reconstituted by the interaction between Mi2G02 and GT-3a, whereas no luciferase signal was observed if Mi2G02 with mutated NLSs or the GUS control was used (Figure 3F). In the Co-IP assay, Mi2G02-HA, HA empty vector or GFP-HA and GT-3a-GFP were co-expressed in *N. benthamiana* leaves. GT-3a-GFP coprecipitated with Mi2G02-HA but not with Mi2G02-mu1-HA, Mi2G02-mu2-HA and Mi2G02-mu3-HA (Figure 3G). There is, therefore, a direct interaction between the nuclear Mi2G02 and *A. thaliana* GT-3a TF *in planta*.

GT-3a is important for *M. incognita* parasitism

GT-3a has been reported to be predominantly expressed in floral buds and roots, especially at the onset of secondary root development (Ayadi et al., 2004). RNA-seq data for *M. incognita*-infected *A. thaliana* galls at 3, 5 and 7 days post inoculation (dpi) and for non-infected roots showed that *GT-3a* was significantly upregulated by nematode infection at these early time points (Yamaguchi et al., 2017). For the analysis of *GT-3a* expression in galls, we cloned a fragment of the GT-3a promoter (-2023 to 0) and transformed *A. thaliana* plants with a *ProGT-3a*:*GUS* fusion. We then inoculated the transformed plants with *M. incognita* and performed histochemical assays. We observed a strong GUS signal in uninfected root vascular tissues and lateral root initials, and in developing galls at 3, 5 and 7 dpi (Figure 4A). These results suggest that *GT-3a* plays a role early in nematode feeding site development.

We explored the biological functions of GT-3a during gall formation in two *gt-3a* T-DNA knockout (KO) mutant *A. thaliana* lines (*SALK_134703* and *SALK_040448*) (Supplemental Figure 4A). We also generated transgenic *A. thaliana* lines overexpressing a GT-3a-GFP fusion and GFP alone. Homozygous KO mutants were verified by PCR and semiquantitative RT-PCR (Supplemental Figure 4B and 4C). Two independent *GT-3a-GFP*-overexpressing lines were selected and verified by semiquantitative RT-PCR, western blotting and observing GFP fluorescence (Supplemental Figure 5D-5F). No macroscopic root phenotype was observed in the two *gt-3a* T-DNA KO lines relative to wild-type Col-0 (Supplemental Figure 4G). As observed for Mi2G02, the two independent *GT-3a-GFP*-overexpressing lines had longer roots (8%; n=10) than the wild-type plants, and also had a larger number (92%

and 87%; *n*=10) of lateral roots and a greater lateral root density than the wild-type plants (Figure 4B and 4C and Supplemental Figure 4H). These lines were then subjected to nematode infection assays. *GT-3a*-overexpressing plants had larger numbers of galls and egg masses (37% and 48%, *n*=18) than control plants (Figure 4D and Supplemental Figure 5A). By contrast, the two *gt-3a* mutants were significantly less susceptible to *M. incognita* than control plants, as shown by their smaller numbers of galls (more than 60% fewer, *n*=26) and the almost complete absence of egg masses (Figure 4E and Supplemental Figure 5B). In these KO lines, the areas covered by GCs were 40% (*n*=10) smaller than those in control plants (Figure 4F). The GT-3a transcription factor, therefore, regulates root development and plays an essential role in GC development and *M. incognita* parasitism.

GT-3a targets and represses *TOZ* and *RAD23C*

We investigated the transcriptional activity of GT-3a, by fusing the *GT-3a* coding sequence to the sequence encoding the GAL4 DNA-binding domain in the pGBKT7 (BD) vector, and using the resulting plasmid to transform the yeast strain AH109. Yeast cells transformed with the positive control pCL-1, encoding the full-length wild-type GAL4 protein, grew well on SD-Trp-His selection medium and displayed X-α-Gal activity (Figure 5A). By contrast, yeast cells harboring BD-GT-3a or the empty BD plasmid (negative control) were unable to grow on SD-Trp-His selection medium (Figure 5A). These results suggest that GT-3a does not act as a transcriptional activator and, therefore, probably acts by repressing gene expression.

We then sought to identify the genes for which expression was modulated by GT-3a, by searching *A. thaliana* promoter sequences for 5'-GTTAC-3' DNA element, which was known to be specifically targeted by GT-3a (Ayadi et al., 2004), and for the 5'-CACGTG-3' DNA element, with the PlantRegMap tool (Tian et al., 2019). Further, we turned to the ePlant online tools and explored the expression patterns of candidate genes under nematode infection and in developing roots (Waese et al., 2017). We retrieved nine putative GT-3a targets (Supplemental Table 2), which were then further studied with a yeast one-hybrid (Y1H) approach. The Y1H assay revealed that GT-3a bound directly to the promoters of *TORMOZ* (*TOZ*; *AT5G16750*), *RADIATION SENSITIVE 23C* (*RAD23C; AT3G02540*) and a WRKY transcription factor (*WRKY2*; *AT5G56270*) (Figure 5B and Supplemental Figure 6).

We investigated the ability of GT-3a to repress the expression of *TOZ, RAD23C* or *WRKY2* in a dual-luciferase reporter assay. A construct expressing *GT-3a* and a

reporter construct consisting of the *TOZ*, *RAD23C* or *WRKY2* promoter driving transcription of the firefly luciferase (*LUC*) reporter gene were used for the co-infiltration of *N. benthamiana* leaves. GT-3a decreased the activity of the *TOZ* and *RAD23C* promoters, measured as a *firefly*-to-*Renilla* (LUC/REN) luciferase ratio, by 30% and 50%, respectively, relative to the GFP control, whereas it did not decrease *WRKY2* promoter activity (Figure 5C). For confirmation of this result, we used RT-qPCR to quantify *TOZ* and *RAD23c* expression in transgenic *A. thaliana* plants overexpressing *GT-3a*. Both *TOZ* and *RAD23c* appeared to be repressed in the two independent transgenic lines relative to the wild type (Figure 5D).

Finally, we produced a recombinant GT-3a protein, which was used in a gel electrophoretic mobility shift assay (EMSA). GT-3a-His significantly decreased the electrophoretic mobility of the *TOZ* and *RAD23C* promoter probes containing GTTAC or CACGTG elements, but had no effect on the mobility of the mutated probes (GTTAC replaced by AAAAA, CACGTG replaced by AAAAAA) (Figure 5E). This result validates the binding of GT-3a to the *TOZ* and *RAD23c* promoters, and indicates that both the GTTAC and CACGTG elements are important for binding.

These results confirm that GT-3a can bind the *TOZ* and *RAD23C* promoters specifically, downregulating the expression of genes driven by these promoters.

Mi2G02 promotes GT-3a function by stabilizing protein level for nematode parasitism

The *toz* mutant is not viable at postembryonic stages (Griffith et al., 2007) and could not, therefore, be tested in interaction with the nematode. We investigated the role of *RAD23C* in the plant response to *M. incognita* parasitism, with a *rad23c* T-DNA KO mutant *A. thaliana* line (*SALK_068091*) obtained from ABRC (Supplemental Figure 7A). Homozygous KO plants were verified by PCR on genomic DNA (Supplemental Figure 7B) and by RT-qPCR on cDNA (Supplemental Figure 7C). No difference in root phenotype was observed between the *rad23c* T-DNA KO line and wild-type plants (Supplemental Figure 7D), consistent with previous reports (Farmer et al., 2010). Following *M. incognita* infection, the *rad23c* KO lines were significantly more susceptible to the nematode than control plants, as shown by the larger numbers of galls (43%, *n*=28), and egg masses (39%) observed (Figure 6A and Supplemental Figure 7E). RAD23C therefore downregulates *M. incognita* parasitism.

We addressed the potential outcome of Mi2G02 binding to GT-3a more precisely, by co-expressing Mi2G02 and GT-3a in *N. benthamiana* leaves and performing dual-

luciferase reporter assays. The previously observed suppression of *TOZ* and *RAD23C* expression mediated by GT-3a was significantly enhanced in the presence of Mi2G02 (Figure 6B). We also performed transient expression assays and western blotting to determine whether Mi2G02 affected the amount of GT-3a protein in *N. benthamiana* agro-infiltrated leaves. The co-expression of Mi2G02 and GT-3a-GFP in *N. benthamiana* leaves resulted in a significant higher GFP fluorescence intensity (500% to 660% higher) compared with the controls using mutant Mi2G02 or MiEFF18 (Figure 6C and Supplemental Figure 8). Similarly, the co-expression of Mi2G02 and GT-3a in *N. benthamiana* leaves resulted in high levels of GT-3a protein accumulation. No such accumulation was observed with empty vector, Mi2G02 mutants or MiEFF18, used as negative controls (Figure 6D and 6E). Furthermore, treatment with a proteasome inhibitor, MG132, inhibited the degradation of GT-3a (Figure 6E), suggesting that Mi2G02 stabilized GT-3a protein level by inhibiting the 26S proteasome-dependent pathway. Together, these results suggest that the Mi2G02 effector helps to stabilize the GT-3a protein, enabling GT-3a to repress the target genes *TOZ* and *RAD23C,* to promote nematode parasitism (Figure 7).

DISCUSSION

Phytopathogen success depends on the secretion of effector proteins to reprogram the host transcriptome to facilitate parasitism. Pathogens have been shown to secrete effectors that can function as TFs or target TFs to manipulate host cell physiology and/or immunity. In plant-nematode interactions, the 10A07 effector from the sugar beet cyst nematode, *Heterodera schachtii*, is expressed in the nematode dorsal gland cell and targets a plant kinase and the IAA16 transcription factor. There is also evidence to suggest that the 10A07-IAA16 interaction interferes with auxin signaling by modulating the expression of several auxin response factors (Hewezi et al., 2015). Nevertheless, the function of nematode nuclear effectors and the ways in which they manipulate their host targets for feeding site initiation and development remain largely elusive. In this study, we characterized the function of a nuclear effector protein, Mi2G02, and identified its plant target for giant cell formation, the nuclear trihelix transcription factor GT-3a.

Trihelix transcription factors (GTs) are unique to plants and have been shown to be involved in embryogenesis and subsequent plant growth and development and in abiotic stresses (Kaplan-Levy et al., 2012). The *A. thaliana AtGT-3b* and the maize

(*Zea mays*) *ZmGT-3b*, of the GT-1 clade, are induced by pathogens (Park et al., 2004; Zhang et al., 2021). We show here that Mi2G02 can interact with the *A. thaliana* GT-1 clade protein AtGT-3a, resulting in the stabilization of this protein. *AtGT-3a* is induced during the development of galls induced by *M. incognita*. Using *A. thaliana* transgenic plants in which *AtGT-3a* expression was suppressed or constitutively induced, we demonstrated that AtGT-3a was important for giant cell development and successful RKN parasitism.

The *de novo* formation of new organs, such as lateral roots, rhizobium-induced nodules or nematode-induced galls from one or a few root cells requires the recruitment of similar developmental programs (Olmo et al., 2020; Soyano et al., 2019; Yamaguchi et al., 2017). Several genes, including *ABERRANT LATERAL ROOT FORMATION 4* (*ALF4*), a *RIBULOSE-PHOSPHATE 3-EPIMERASE* (*RPE*) and *YUCCA4* (*YUC4*), have been reported to have functions associated with lateral root initiation and/or development and expression regulated in nematode-induced galls; they have also been shown to be required for normal feeding site formation and nematode development (Favery et al., 1998; Olmo et al., 2019; Suzuki et al., 2022). These genes include cell-cycle genes and TF genes, such as *LBD16* and *PUCHI,* that play key roles in controlling lateral root initiation and morphogenesis (Torres-Martínez et al., 2019), and are induced following nematode infection and required for feeding site development and successful RKN parasitism (Cabrera et al., 2014; Suzuki et al., 2021). Similarly, *Medicago truncatula LBD16* mutants display nodule initiation defects on inoculation with *Sinorhizobium meliloti* (Schiessl et al., 2019). The rewiring of transcriptional networks to alter root system architecture also involves changes in endogenous levels of growth-related plant hormones, and the production of phytohormones or deployment of hormone-mimicking strategies by symbiotic and parasitic microbes (Eichmann et al., 2021; Gheysen and Mitchum, 2019). We show here that the expression of *Mi2G02* in *A. thaliana* can promote root growth and the development of giant cells, and that Mi2G02 acts by stabilizing AtGT-3a, with mutations of the gene encoding this transcription factor also impairing giant cell formation. *AtGT-3a* was found to be strongly induced at the onset of lateral root development (this study and (Ayadi et al., 2004). AtGT-3a therefore seems to be one of the TFs regulating both lateral root development and nematode-feeding site neo-organogenesis.

The binding of GT-3a to the promoter of the *TOZ* and *RAD23C* genes was confirmed by Y1H and EMSA assays. TOZ is a predicted WD40 repeat protein involved in the regulation of cell division planes and the expression of patterning genes during embryogenesis. It may, therefore be involved in plant embryogenesis and organogenesis, including root development (Griffith et al., 2007), suggesting a possible role in the regulation of root-knot neo-organogenesis. RAD23 probably acts as a shuttle protein, delivering ubiquitinated substrates to the ubiquitin/26S proteasome system for degradation. Roles in plant processes as diverse as the cell cycle, cell morphogenesis, and flower development have been proposed for RAD23 (Farmer et al., 2010; Maclean et al., 2014). Interestingly, a role for RAD23 proteins in plant immunity has been proposed, probably through interactions with stress-associated proteins (SAPs) acting as ubiquitin E3 ligases (Kang et al., 2017; Liu et al., 2019). Consistently, RAD23 proteins have been shown to be targeted by plant pathogen effectors, possibly to modulate host protein degradation and suppress host defense responses. The *A. thaliana* RAD23A was identified as a putative target of the *Pseudomonas syringae* HopM1 effector (Nomura et al., 2006), and the phytoplasma SAP54 effector was shown to interact with both RAD23C and RAD23D (Maclean et al., 2014). Intriguingly, a previous report confirmed that RAD23 proteins associated with the 26S proteasome and played an essential role in the cell cycle (Farmer et al., 2010), roles of GT-3a and *RAD23C* in proteolysis and cell fate determination are expected. In support of this, the transcription activity assays performed in yeast and *in planta* demonstrated that GT-3a downregulated expression of the *TOZ* and *RAD23C* genes, which suppression was enhanced by co-expressing with Mi2G02. Moreover, Mi2G02 stabilized GT-3a protein level by inhibiting the 26S proteasome-dependent pathway. Using *rad23c* KO *A. thaliana* lines, we showed that *RAD23C* inactivation increased susceptibility to RKNs, demonstrating that *RAD23C* is a key gene for plant-nematode interactions.

It has been suggested that Mj2G02 interferes with both jasmonate signaling and plant immune responses (Song et al., 2021). Mj2G02 expression *in planta* resulted in the accumulation of jasmonoyl-isoleucine, the endogenous bioactive form of jasmonate (JA), in transgenic *A. thaliana*, and a dysregulation of the expression of *JASMONATE ZIM DOMAIN* (*JAZ*) transcriptional repressors and jasmonate-responsive genes (Song et al., 2021). Our data indicate that Mi2G02 could divert the host plant developmental program to promote the formation of the feeding sites

important for nematode development and reproduction. RKNs may secrete the 2G02 effector to stabilize GT-3a, maintaining the concentration of this TF at a sufficiently high level to repress the growth regulator genes, *TOZ* and *RAD23c*, thereby promoting GC development. We hypothesise that, as previously suggested for ZmGT-3a (Zhang et al., 2021), GT-3a acts at the interface between growth and immunity. Microbes can interfere with central regulators of root cell identity and root growth that are also involved in the response to biotic stress (Rich-Griffin et al., 2020; üstüner et al., 2022). Plant hormones, the signaling pathways of which may interact at central hubs, also regulate growth-immunity tradeoffs (Guo et al., 2018; Huot et al., 2014). For instance, cross-talk between gibberellin (GA)-mediated growth and JA-mediated defense signaling pathways participates contributes to maintaining the balance between growth and immunity (Huot et al., 2014; Pieterse et al., 2014). DELLA proteins repress growth-related TFs unless they are degraded in the presence of growth-promoting GA. DELLA also binds to JAZs, and DELLA degradation allows JAZs to interact with their cognate TFs, thereby decreasing JA-dependent signaling. Treatment with flg22 suppresses GA-mediated DELLA degradation, leading to an inhibition of root growth dependent on salicylic acid (SA), an antagonist of the JA signaling pathway (Huot et al., 2014; Pieterse et al., 2014). JA is a known growth inhibitor that stabilizes DELLA and has been shown to downregulate the cyclin-dependent kinases CDKA1 and CYCB1;1 required for cell-cycle progression (Qi and Zhang, 2020; Reitz et al., 2015). Biotic stress may, therefore, affect cell cycle regulators, and cell division and hormones influence the underlying regulatory mechanisms.

The plant response to pathogens is highly dependent on the interplay between immunity and development. Regulators of cell identity and TFs may play a crucial role in connecting the developmental and immunity gene networks to reflect response specificity (Rich-Griffin et al., 2020). By modulating GT-3a TF availability in plant cells, the RKN effector 2G02 can alter both the root developmental program and JA-dependent signaling pathways to allow giant cell formation and successful parasitism. In this respect, GT-3a constitutes a novel example of a key regulator recruited by a biotrophic pathogen at the interface between growth and immunity.

METHODS

Nematodes and plant materials

Meloidogyne incognita was reproduced on tomato plants (*Solanum lycopersicum* var. 'Moneymaker'). Egg masses and preparasitic second-stage juveniles (pre-J2s) were collected as previously described (Zhao et al., 2019). *Arabidopsis thaliana* seeds were germinated on Murashige and Skoog (MS) medium (Coolaber, Cat. No. PM1012) at 25°C in a growth chamber and the seedlings were transplanted into pots of soil at 13 days. The *gt-3a* T-DNA mutant lines (*SALK_014703* and *SALK_040448*), and the *At3g02540* (*rad23c*) T-DNA mutant line (*SALK_068091*) were obtained from the Arabidopsis Biological Resource Center (ABRC, USA). The homozygous plants were verified by PCR and semiquantitative RT-PCR. *Nicotiana benthamiana* plants and *A. thaliana* plants were grown in pots and placed in a culture room at a temperature of 23°C, with a 16 h light/8 h dark photoperiod, with fluorescent bulbs used to generate soft white light.

Nematode infections and gall sections

A. thaliana seedlings (one month after transplanting) were inoculated with pre-J2s. For nematode susceptibility assays, *A. thaliana* roots were inoculated with 200 pre-J2s per plant. The roots were collected and galls and egg masses were counted under a dissecting microscope (Olympus, Japan) 35 days post inoculation (dpi). For gall collection, roots were inoculated with 500 pre-J2s per plant. Galls were collected at 3 dpi, 5 dpi, 7 dpi, 14 dpi and 21 dpi and fixed as previously described (Gavrilovic et al., 2016). At least 10 galls were fixed for each *A. thaliana* line. Gall sections were stained with 0.05% toluidine blue and photographed on a Zeiss microscope (Zeiss AxioImager Z2, Germany). The areas of the giant cells were measured with ImageJ software (Schindelin et al., 2012). Generally, the first step is to open the program and draw a line as the same with image scale, then go to 'Analyze', 'Set Scale' and enter the values: 'known distance' is 100, and 'Unit of length' is 'μm', select 'Global' and click 'OK'. The second step is to go to 'Analyze', 'Set Measurements', select 'Area' and click 'OK'. The third step is to select 'Freehand selections', select giant cell area, go to 'Analyze', select 'Measure' and click 'OK'.

DNA/RNA isolation and gene amplification

M. incognita RNA was extracted with TRIzol reagent (Invitrogen, USA, Cat. No. 10296010) as previously described (Lin et al., 2013; Zhao et al., 2021). Total RNA was extracted from *A. thaliana* seedlings (ten days after germination) with the RNAprep Pure Plant Kit (TIANGEN, Cat. No. DP432), according to the manufacturer's instructions. The RNA was then used for cDNA synthesis with the M-MLV reverse

transcriptase (TaKaRa, Cat. No. 2641Q) in accordance with the manufacturer's instructions. DNA was extracted with the Plant Genomic DNA Kit (TIANGEN, Cat. No. DP305) according to the manufacturer's instructions. Gene and promoter sequences were amplified from cDNA or gDNA by PCR with specific primers. All the primers used in this study are provided in Supplemental Table S3 and were synthesized by TsingKe Biotechnology Co. Ltd, Beijing, China.

RT-qPCR analysis

RNA was extracted and cDNA was synthesized for reverse transcription-quantitative PCR (RT-qPCR), with the BIO-RAD CFX96 (BIO-RAD, USA) real-time PCR system, as follows: 95 °C for 5 min and 40 cycles of 95 °C for 30 s and 60 °C for 30 s. The data were analyzed with the $2^{-\Delta\Delta CT}$ method (Livak and Schmittgen, 2001). For internal controls, *M. incognita GAPDH* (*Minc12412*) or *A. thaliana UBP22* (*AT5G10790*) was used for the normalization of RT-qPCR data. RT-qPCR assays were repeated three times.

Plasmid construction and plant transformation

For RNAi experiments in *A. thaliana*, a 204-nucleotide *Mi2G02* fragment was amplified and inserted upstream and downstream from the pSAT5 intron in the forward and reverse orientations (Dafny-Yelin et al., 2007), and then inserted into the pSUPER destination vector, to construct pSUPER-Mi2G02-RNAi.

A signal peptide-deficient *Mi2G02* sequence and ShKT domain were amplified by PCR and inserted into the Super-GFP (C-terminal GFP) to generate Super-Mi2G02-GFP and Super-Mi2G02-ShkT-GFP. The nuclear localization sequences of *Mi2G02* were mutated and inserted into Super-GFP vector to generate Super-Mi2G02-mu1-GFP, Super-Mi2G02-mu2-GFP and Super-Mi2G02-mu3-GFP. The ORF of *GT-3a* was inserted into the pBin-mcherry (N-terminal mcherry) vector to generate pBin-mcherry-GT-3a. Plasmids were checked by sequencing and used to transform *A. tumefaciens* strain GV3101.

For ectopic expression in *A. thaliana*, the *Mi2G02* (without signal peptide sequences) and *AT5G01380* (*GT-3a*) ORFs were amplified and the corresponding PCR fragments were inserted into the Super-HA vector (C-terminal HA tag) and the Super-GFP (C-terminal GFP tag) vector to construct Super-Mi2G02-HA and Super-GT-3a-GFP, respectively. The plasmids were verified by sequencing and used to transform *A. tumefaciens* GV3101, with empty vectors used as a control.

For the yeast two-hybrid (Y2H) screens, *Mi2G02* (lacking the signal peptide sequence) was amplified and inserted into the pGBKT7 (BD) vector. For pairwise Y2H verification, the coding sequences of *AT5G01380* (*GT-3a*), *AT3G52590* and *AT3G02550* were inserted into the pGADT7 (AD) vector. For identification of the key domains for interaction, *Mi2G02-ShKT* (Mi2G02 retaining the ShKT domain) and *Mi2G02-ΔShKT* (Mi2G02 without the ShKT domain) were amplified and inserted into BD vectors, and *GT-3a-DB* (GT-3a retaining the DNA-binding domain) and *GT-3a-ΔDB* (GT-3a lacking the DNA-binding domain) were inserted into AD vectors. The plasmids were verified by sequencing and used to transform Y2HGold competent yeast cells.

For the yeast one-hybrid (Y1H) assay, the coding region of *GT-3a* was amplified and inserted into the pB42AD vector. Fragments of candidate promoters were amplified and inserted into the pLacZi vector.

For the bimolecular fluorescence complementation (BiFC) assay, *Mi2G02* (lacking the signal peptide sequence) and *GT-3a* coding sequences were inserted into the nE-YFP and cE-YFP vectors (Walter et al., 2004), respectively.

For the luciferase complementation assay (LCA), the full-length coding sequence of *Mi2G02* (lacking the signal peptide sequence) or *GT-3a* was inserted into the pCAMBIA1300-nLUC or pCAMBIA1300-cLUC vector. The plasmids were verified by sequencing and used to transform *A. tumefaciens* GV3101.

For the co-immunoprecipitation (Co-IP) assay, the coding regions of *Mi2G02* (lacking the signal peptide sequence) or *GT-3a* were inserted into the super1300 vectors with an HA-tag and a FLAG-tag, respectively, fused to the C-terminal end of the sequence. Plasmids were verified by sequencing and used to transform *A. tumefaciens* GV3101.

For GUS-staining assays, a 2023 bp fragment of the *GT-3a* promoter was inserted into the pBI101 vector to generate *ProGT-3a*:*GUS*. The resulting plasmid was verified by sequencing and used to transform *A. tumefaciens* GV3101.

For dual-luciferase reporter assays, the coding sequence of *GT-3a* was amplified and inserted into the pCAMBIA3301 vector to generate pCAMBIA3301-GT-3a. A 623 bp fragment upstream from the start codon of *TOZ* and a 595 bp fragment upstream from the start codon of *RAD23C* were amplified and inserted into the pro-LUC-*35S*-Rluc vector to generate *TOZpro*-LUC-*35S*-Rluc and *RAD23Cpro*-LUC-*35S*-Rluc,

respectively. The plasmids were verified by sequencing and used to transform *A. tumefaciens* strain GV3101.

A recombinant GT-3a protein was produced by amplifying the coding sequence of *GT-3a* and inserting it into the pET30a vector (C-terminal His tag) to generate pET30a-GT-3a. The resulting plasmid was verified by sequencing and used to transform *Escherichia coli* strain BL21 (DE3) cells.

The primers (synthesized by Tsingke Biotechnology Co., Ltd., Beijing, China) and restriction enzymes (NEB, MA, USA) used for plasmid construction are listed in Supplemental Table 3.

Generation of transgenic *A. thaliana* plants and nematode infection assays

The sequenced pSUPER-Mi2G02-RNAi, Super1300-Mi2G02-HA, Super1300-GT-3a-GFP and Super1300-GFP plasmids were used to transform *A. tumefaciens* strain *GV3101*. Four-week old *A. thaliana* plants were transformed with *A. tumefaciens* by the floral dip method (Clough and Bent, 1998). *A. thaliana* lines were confirmed to be homozygous for the transgene by qPCR and/or western blotting. Nematode infection assays were performed three times.

Subcellular localization assay

Four-week-old *N. benthamiana* leaves were infiltrated with *A. tumefaciens* carrying the appropriate plasmids in infiltration buffer (10 mM $MgCl_2$, 10 mM MES, and 0. 1mM AS) at an OD_{600} of 0.4. Images were captured by laser confocal fluorescence microscopy (Zeiss LSM700, Germany) 2 dpi, at an excitation wavelength of 488 nm for GFP and 561 nm for mcherry.

Yeast two-hybrid (Y2H) and yeast one-hybrid (Y1H) assays

A cDNA library was constructed by extracting RNA from *A. thaliana* roots infected with *M. incognita* (1 dpi, 3 dpi, 5 dpi, 10 dpi, 14 dpi) and using it to screen for the target proteins of Mi2G02. The Y2H assay was performed according to the Clontech protocol (Clontech, USA). Interactions between Mi2G02 and candidate proteins were assessed in pairwise Y2H assays. Relative BD and AD vectors were used to transform the yeast strain Y2HGold for screening on SD/-Leu-Trp plates. Positive clones were verified and selected for culture on SD/-Leu-Trp-His medium supplemented with 20 mg/mL 5-bromo-4-chloro-3-indolyl-α-D-galactopyranoside (X-α-Gal; Coolaber, Cat. No. SL0940). We investigated the requirement of the nuclear localization sequences of *Mi2G02* for interaction by inserting a mutated *Mi2G02* in the BD vector for pairwise Y2H assays.

The Y1H assay was performed as previous described (Kong et al., 2023). The sequenced pB42AD and pLacZi vectors were integrated into the yeast strain EGY48 grown on the SD/-Trp-Ura medium (Coolaber, Cat. No. PM2262). Positive transformants were verified and selected for growth on medium containing raffinose (Coolaber, Cat. No. SL0990), and 5-bromo-4-chloro-3-indolyl-b-D-galactopyranoside (X-gal, Coolaber, Cat. No. CX11921) for color reactions.

Bimolecular fluorescence complementation (BiFC) assay

BiFC assays were performed as previously described (Zhao et al., 2019). *Agrobacterium* harboring appropriate pairs of vectors was infiltrated into *N. benthamiana* leaves for 48 h. YFP fluorescence, indicating protein interaction, was captured with a confocal microscope (Zeiss LSM700, Germany) with excitation at 514 nm and emission at 527 nm.

Luciferase complementation assay

Agrobacterium cultures were resuspended in infiltration buffer, incubated at room temperature for 3 h, and then infiltrated into four-week old *N. benthamiana* leaves. Three days after agro-infiltration, 1 mM luciferin (Biovision, Cat. No. 7903) solution was sprayed onto the infiltrated leaves, and luciferase activity was detected with a low-light cooled CCD imaging apparatus ChemiScope 6000 (Clinx Science Instruments Co., Ltd, Shanghai, China).

***In vivo* co-immunoprecipitation (Co-IP) assay**

Total protein was extracted from four-week-old *N. benthamiana* leaves co-expressing Mi2G02 and GT-3a, after 48 h of infiltration. Co-IP was performed with BeyoMag™ Anti-HA Magnetic Beads (Beyotime, Cat. No. P2121) as previously described (Zhao et al., 2021). The eluted proteins were checked by western blotting with anti-GFP (ABclonal, Cat. No. AE012) and anti-HA (Coolaber, Cat. No. AB1105) antibodies, respectively.

Histochemical analysis of GUS activities

Transgenic *A. thaliana* was generated as described above. The homozygosity of the transgenic lines was confirmed by PCR and they were inoculated with *M. incognita*. Root samples were collected at 3 dpi, 5 dpi, 7 dpi, and 14 dpi. More than 10 roots were collected at each sampling time. Histochemical staining for GUS enzyme activity was performed with a GUS staining kit (Coolaber, Cat. No. SL7160), in accordance with the manufacturer's instructions. Images were captured with a stereomicroscope (Zeiss, AxioImager Z2, Germany).

Dual-luciferase reporter assay

Agrobacterium harboring pCAMBIA3301-GT-3a was infiltrated with *TOZpro*-LUC-*35S*-Rluc or *RAD23Cpro*-LUC-*35S*-Rluc, with or without Mi2G02, into four-week-old *N. benthamiana* leaves. Three days after infiltration, leaf discs with a diameter of 2 cm were harvested and ground in liquid nitrogen. Firefly and Renilla luciferase activities were measured with a Dual-Luciferase Reporter Assay System (Vazyme, Cat. No. DL101-01) according to the manufacturer's instructions, with Synergy SLXFA (BioTek, USA).

Electrophoretic mobility shift assay (EMSA)

The recombinant GT-3a-His protein was induced with 1 mM isopropyl-β-d-thiogalactoside (IPTG) and purified with the His-tag Protein Purification Kit (Beyotime, Cat. No. P2229S) according to the manufacturer's instructions (Zhao et al., 2021). The biotin-labeled and unlabeled probes for *TOZ* and *RAD23C,* containing the -GTTAC- element or the -CACGTG- element, were synthesized and purified by Sangon Biotech (Shanghai, China). EMSA was carried out with an EMSA chemiluminescence kit (Beyotime, Cat. No. GS009). Competition experiments were performed with various amounts of unlabeled oligonucleotides. The mutated competitor was generated by replacing five base pairs or six base pairs in the *TOZ* and *RAD23C* binding elements (GTTAC to AAAAA or CACGTG to AAAAAA). EMSA assays were repeated three times.

Transient expression assays in *N. benthamiana* leaves

Four-week-old *N. benthamiana* leaves were infiltrated with *A. tumefaciens* carrying the appropriate plasmids in infiltration buffer (10 mM $MgCl_2$, 10 mM MES, and 0. 1mM AS) at an OD_{600} of 0.4. MG132 (100 μM) was added 24 h before protein extraction.

Cell fractionation, protein extraction and western blotting

Cell fractionation assay was followed as described previously (Wang et al., 2018) with some modifications. Briefly, *N. benthamiana* leaves expressing proper proteins (0.5 g) were harvested and ground in liquid nitrogen and mixed with 2 mL/g of lysis buffer (20 mM Tris-HCl, pH 7.5, 20 mM KCl, 2 mM EDTA, 2.5 mM $MgCl_2$, 25% glycerol, 250 mM sucrose, and 5mM DTT) supplemented with protease inhibitor cocktail (Beyotime, Cat. No. P1045). The homogenate was filtered through a double layer of Miracloth (Millipore, Cat. No. 475855). The flow-through was centrifuged at 1500g for 10 min at 4°C, and the supernatant, consisting of the cytoplasmic fraction, was centrifuged at 10,000g for 10 min at 4°C, and was collected as the cytoplasmic fraction. The pellet

from the first centrifugation was washed four times with 4 mL NRBT buffer (20 mM Tris-HCl, pH7.5, 2.5 mM $MgCl_2$, 25% glycerol, and 0.2% TritonX-100) and then resuspended with 500 µL of NRB2 (20 mM Tris-HCl, pH 7.5, 10 mM $MgCl_2$, 0.25 M sucrose, 0.5% Triton X-100, and 5 mM β-mercaptoethanol) supplemented with protease inhibitor cocktail and carefully overlaid on top of 500 µL of NRB3 (20 mM Tris-HCl, 10 mM MgCl2, pH 7.5, 1.7 M sucrose, 0.5% Triton X-100, and 5 mM β-mercaptoethanol) supplemented with protease inhibitor cocktail. The suspension was centrifuged at 16,000g for 45 min at 4°C, and the pellet was collected as the nuclear fraction. The 2× SDS loading buffer was then added to the cytoplasmic and nuclear fractions and boiled for 5 min. Actin was detected with an anti-actin antibody (ABclonal, Cat. No. AC009) as a cytoplasmic marker. H3 proteins were detected using an anti-H3 antibody (ABclonal, Cat. No. A2348) as a nuclear marker. Total proteins were extracted from *N. benthamiana* leaves or *A. thaliana* seedlings (ten days after germination) in RIPA lysis buffer (Beyotime, Cat. No. P0031K) supplemented with protease inhibitor cocktail. For tag antibodies, we used anti-His (TransGen, Cat. No. HT501), anti-GFP (ABclonal, Cat. No. AE012), and anti-HA (Coolaber, Cat. No. AB1105) antibodies, and a goat anti-mouse IgG (H+L)-HRP-conjugated secondary antibody (Coolaber, Cat. No. AB2102). The protein was detected with the EasySee Western Blot Kit (TransGen, Cat. No. DW101). Band intensity was determined by ImageJ software.

Statistical methods

The significance of differences between two groups was assessed in two-tailed *t*-tests. For multiple comparisons, the significance of differences was assessed by one-way ANOVA followed by Tukey tests for multiple comparisons. All statistical analyses were performed with GraphPad Prism software version 8.3.0.

Accession numbers

The accession numbers of major genes mentioned in this study are as follows: *Mi2G02* (*AAQ10016*), *GAPDH* (*Minc12412*), *GT-3a* (*AT5G01380*), *LBD41* (*AT3G02550*), *UBQ1* (*AT3G52590*), *TOZ* (*AT5G16750*), *RAD23C* (*AT3G02540*), *WRKY2* (*AT5G56270*), *UBP22* (*AT5G10790*), *SRP34* (*AT1G02840*), *DVL4* (*AT1G13245*), *SKP2* (*AT1G21410*), *FEI1* (*AT1G31420*), *FEI2* (*AT2G35620*), *ABS4* (*AT1G58340*).

DATA AVAILABILITY

All relevant data is included in the main manuscript and the Supplemental Information.

AUTHOR CONTRIBUTIONS

J.Z., B.F., P.A., M.Q., H.J. and Z.M. conceived the project. J.Z., K.H., B.F., Y.L., J.L. and Y.Y. designed and planned the experiments. J.Z., K.H., R.L., and Y.L. performed the experiments and collected and analyzed the data. J.Z., B.F., P.A. and M.Q. wrote the manuscript.

ACKNOWLEDGEMENTS

This research supported by the Youth Innovation Program of the Chinese Academy of Agricultural Sciences (Grant No. Y2022QC06), the National Natural Science Foundation of China (Grant Nos. 32001878, 32172366), the Natural Science Foundation of Beijing (Grant No. 6222054), the China Agriculture Research System (CARS-23), and the French Government (National Research Agency, ANR) through the 'Investments for the Future' LabEx SIGNALIFE (#ANR-11-LABX-0028-01), IDEX UCAJedi (#ANR-15-IDEX-0). We thank Dr Panpan Yang (Institute of Vegetables and Flowers, Chinese Academy of Agricultural Science, Beijing, China) for providing the CP516 vector and the p3301 vector, Dr Jinzhuo Jian (Institute of Plant Protection, Chinese Academy of Agricultural Science, Beijing, China) for advice concerning gall sections, and Dr Qian Wei (the Core Facility Platform, Institute of Crop Sciences, Chinese Academy of Agricultural Sciences, Beijing, China) for assistance with confocal microscopy.

COMPETING INTERESTS

The authors declare no competing interests.

REFERENCES

Abad, P., Gouzy, J., Aury, J., Castagnone-Sereno, P., Danchin, E.G.J., Deleury, E., Perfus-Barbeoch, L., Anthouard, V., Artiguenave, F., and Blok, V.C., et al. (2008). Genome sequence of the metazoan plant-parasitic nematode *Meloidogyne incognita*. *Nature Biotechnology* **26**:909-915. 10.1038/nbt.1482.

Ayadi, M., Delaporte, V., Li, Y., and Zhou, D. (2004). Analysis of GT-3a identifies a distinct subgroup of trihelix DNA-binding transcription factors in *Arabidopsis*. *FEBS*

Letters **562**:147-154. 10.1016/S0014-5793(04)00222-4.

Baldacci-Cresp, F., Behr, M., Kohler, A., Badalato, N., Morreel, K., Goeminne, G., Mol, A., de Almeida Engler, J., Boerjan, W., and El Jaziri, M., et al. (2020). Molecular changes concomitant with vascular system development in mature galls induced by root-knot nematodes in the model tree host *Populus tremula* × *P. alba*. *International Journal of Molecular Sciences* **21**:406. 10.3390/ijms21020406.

Barcala, M., García, A., Cabrera, J., Casson, S., Lindsey, K., Favery, B., García-Casado, G., Solano, R., Fenoll, C., and Escobar, C. (2010). Early transcriptomic events in microdissected Arabidopsis nematode-induced giant cells. *Plant Journal* **61**:698-712. 10.1111/j.1365-313X.2009.04098.x.

Bartlem, D.G., Jones, M.G.K., and Hammes, U.Z. (2014). Vascularization and nutrient delivery at root-knot nematode feeding sites in host roots. *Journal of Experimental Botany* **65**:1789-1798. 10.1093/jxb/ert415.

Cabrera, J., Barcala, M., Fenoll, C., and Escobar, C. (2014). Transcriptomic signatures of transfer cells in early developing nematode feeding cells of Arabidopsis focused on auxin and ethylene signaling. *Frontiers in Plant Science* **5**:107. 10.3389/fpls.2014.00107.

Cabrera, J., Díaz Manzano, F.E., Sanchez, M., Rosso, M.N., Melillo, T., Goh, T., Fukaki, H., Cabello, S., Hofmann, J., and Fenoll, C., et al. (2014). A role for *LATERAL ORGAN BOUNDARIES-DOMAIN 16* during the interaction *Arabidopsis-Meloidogyne* spp. provides a molecular link between lateral root and root-knot nematode feeding site development. *New Phytologist* **203**:632-645. 10.1111/nph.12826.

Caillaud, M., Dubreuil, G., Quentin, M., Perfus-Barbeoch, L., Lecomte, P., de Almeida Engler, J., Abad, P., Rosso, M., and Favery, B. (2008). Root-knot nematodes manipulate plant cell functions during a compatible interaction. *Journal of Plant Physiology* **165**:104-113. 10.1016/j.jplph.2007.05.007.

Chhabra, S., Chang, S.C., Nguyen, H.M., Huq, R., Tanner, M.R., Londono, L.M., Estrada, R., Dhawan, V., Chauhan, S., and Upadhyay, S.K., et al. (2014). Kv1.3 channel-blocking immunomodulatory peptides from parasitic worms: implications for autoimmune diseases. *The FASEB Journal* **28**:3952-3964. 10.1096/fj.14-251967.

Clough, S.J., and Bent, A.F. (1998). Floral dip: a simplified method for *Agrobacterium*-mediated transformation of *Arabidopsis thaliana*. *Plant Journal* **16**:735-743. 10.1046/j.1365-313x.1998.00343.x.

Dafny-Yelin, M., Chung, S., Frankman, E.L., and Tzfira, T. (2007). pSAT RNA interference vectors: A modular series for multiple gene down-regulation in plants. *Plant Physiology* **145**:1272-1281. 10.1104/pp.107.106062.

Eichmann, R., Richards, L., and Schäfer, P. (2021). Hormones as go-betweens in plant microbiome assembly. *Plant Journal* **105**:518-541. 10.1111/tpj.15135.

Escobar, C., Brown, S., and Mitchum, M.G. (2011) Transcriptomic and Proteomic Analysis of the Plant Response to Nematode Infection. In: Genomics and molecular genetics of plant-nematode interactions--Jones, J., Gheysen, G., and Fenoll, C.C., ed.eds. Dordrecht: Springer Netherlands. 157-173. 10.1007/978-94-007-0434-3_9.

Farmer, L.M., Book, A.J., Lee, K., Lin, Y., Fu, H., and Vierstra, R.D. (2010). The RAD23 family provides an essential connection between the 26S proteasome and ubiquitylated proteins in *Arabidopsis*. *The Plant Cell* **22**:124-142. 10.1105/tpc.109.072660.

Favery, B., Dubreuil, G., Chen, M., Giron, D., and Abad, P. (2020). Gall-inducing parasites: Convergent and conserved strategies of plant manipulation by insects and nematodes. *Annual Review of Phytopathology* **58**:1-22. 10.1146/annurev-phyto-010820-012722.

Favery, B., Lecomte, P., Gil, N., Bechtold, N., Bouchez, D., Dalmasso, A., and Abad, P. (1998). RPE, a plant gene involved in early developmental steps of nematode feeding cells. *EMBO Journal* **17**:6799-6811. 10.1093/emboj/17.23.6799.

Fuller, V.L., Lilley, C.J., Atkinson, H.J., and Urwin, P.E. (2007). Differential gene expression in Arabidopsis following infection by plant-parasitic nematodes *Meloidogyne incognita* and *Heterodera schachtii*. *Molecular Plant Pathology* **8**:595-609. 10.1111/j.1364-3703.2007.00416.x.

Gavrilovic, S., Yan, Z., Jurkiewicz, A.M., Stougaard, J., and Markmann, K. (2016). Inoculation insensitive promoters for cell type enriched gene expression in legume roots and nodules. *Plant Methods* **12**:4. 10.1186/s13007-016-0105-y.

Gheysen, G., and Mitchum, M.G. (2019). Phytoparasitic nematode control of plant hormone pathways. *Plant Physiology* **179**:1212-1226. 10.1104/pp.18.01067.

Griffith, M.E., Mayer, U., Capron, A., Ngo, Q.A., Surendrarao, A., McClinton, R., Jürgens, G., and Sundaresan, V. (2007). The *TORMOZ* gene encodes a nucleolar protein required for regulated division planes and embryo development in *Arabidopsis*. *The Plant Cell* **19**:2246-2263. 10.1105/tpc.106.042697.

Guo, Q., Major, I.T., and Howe, G.A. (2018). Resolution of growth-defense conflict:

762 mechanistic insights from jasmonate signaling. *Current Opinion in Plant Biology*
763 **44**:72-81. 10.1016/j.pbi.2018.02.009.
764 **Hewezi, T., Juvale, P.S., Piya, S., Maier, T.R., Rambani, A., Rice, J.H., Mitchum,**
765 **M.G., Davis, E.L., Hussey, R.S., and Baum, T.J.** (2015). The cyst nematode
766 effector protein 10A07 targets and recruits host posttranslational machinery to
767 mediate its nuclear trafficking and to promote parasitism in Arabidopsis. *The Plant*
768 *Cell* **27**:891-907. 10.1105/tpc.114.135327.
769 **Hewitson, J.P., Ivens, A.C., Harcus, Y., Filbey, K.J., McSorley, H.J., Murray, J.,**
770 **Bridgett, S., Ashford, D., Dowle, A.A., and Maizels, R.M.** (2013). Secretion of
771 protective antigens by tissue-stage nematode larvae revealed by proteomic analysis
772 and vaccination-induced sterile immunity. *Plos Pathogens* **9**:e1003492.
773 10.1371/journal.ppat.1003492.
774 **Huang, G., Dong, R., Allen, R., Davis, E.L., Baum, T.J., and Hussey, R.S.** (2006).
775 A root-knot nematode secretory peptide functions as a ligand for a plant transcription
776 factor. *Molecular Plant-Microbe Interactions* **19**:463. 10.1094/MPMI-19-0463.
777 **Huang, G., Gao, B., Maier, T., Allen, R., Davis, E.L., Baum, T.J., and Hussey, R.S.**
778 (2003). A profile of putative parasitism genes expressed in the esophageal gland
779 cells of the root-knot nematode *Meloidogyne incognita*. *Molecular Plant-Microbe*
780 *Interactions* **16**:376-381. 10.1094/MPMI.2003.16.5.376.
781 **Huot, B., Yao, J., Montgomery, B.L., and He, S.Y.** (2014). Growth-defense tradeoffs
782 in plants: A balancing act to optimize fitness. *Molecular Plant* **7**:1267-1287.
783 10.1093/mp/ssu049.
784 **Jammes, F., Lecomte, P., Almeida-Engler, J., Bitton, F., Martin-Magniette, M.,**
785 **Renou, J.P., Abad, P., and Favery, B.** (2005). Genome-wide expression profiling
786 of the host response to root-knot nematode infection in Arabidopsis. *Plant Journal*
787 **44**:447-458. 10.1111/j.1365-313X.2005.02532.x.
788 **Jones, J.T., Haegeman, A., Danchin, E.G.J., Gaur, H.S., Helder, J., Jones, M.G.K.,**
789 **Kikuchi, T., Manzanilla-López, R., Palomares-Rius, J.E., and Wesemael,**
790 **W.M.L., et al.** (2013). Top 10 plant-parasitic nematodes in molecular plant
791 pathology. *Molecular Plant Pathology* **14**:946-961. 10.1111/mpp.12057.
792 **Joshi, I., Kumar, A., Kohli, D., Bhattacharya, R., Sirohi, A., Chaudhury, A., and**
793 **Jain, P.K.** (2022). Gall-specific promoter, an alternative to the constitutive
794 *CaMV35S* promoter, drives host-derived RNA interference targeting *Mi-msp2* gene
795 to confer effective nematode resistance. *Frontiers in Plant Science* **13**:1007322.

10.3389/fpls.2022.1007322.

Joshi, I., Kumar, A., Singh, A.K., Kohli, D., Raman, K.V., Sirohi, A., Chaudhury, A., and Jain, P.K. (2019). Development of nematode resistance in Arabidopsis by HD-RNAi-mediated silencing of the effector gene *Mi-msp2*. *Scientific Reports* **9**:17404. 10.1038/s41598-019-53485-8.

Kang, M., Lee, S., Abdelmageed, H., Reichert, A., Lee, H.K., Fokar, M., Mysore, K.S., and Allen, R.D. (2017). Arabidopsis stress associated protein 9 mediates biotic and abiotic stress responsive ABA signaling via the proteasome pathway. *Plant, Cell and Environment* **40**:702-716. 10.1111/pce.12892.

Kaplan-Levy, R.N., Brewer, P.B., Quon, T., and Smyth, D.R. (2012). The trihelix family of transcription factors-light, stress and development. *Trends in Plant Science* **17**:163-171. 10.1016/j.tplants.2011.12.002.

Kong, D., Li, C., Xue, W., Wei, H., Ding, H., Hu, G., Zhang, X., Zhang, G., Zou, T., and Xian, Y., et al. (2023). UB2/UB3/TSH4-anchored transcriptional networks regulate early maize inflorescence development in response to simulated shade. *The Plant Cell* **35**:717-737. 10.1093/plcell/koac352.

Lin, B., Zhuo, K., Wu, P., Cui, R., Zhang, L., and Liao, J. (2013). A novel effector protein, MJ-NULG1a, targeted to giant cell nuclei plays a role in *Meloidogyne javanica* parasitism. *Molecular Plant-Microbe Interactions* **26**:55. 10.1094/MPMI-05-12-0114-FI.

Liu, S., Yuan, X., Wang, Y., Wang, H., Wang, J., Shen, Z., Gao, Y., Cai, J., Li, D., and Song, F. (2019). Tomato stress-associated protein 4 contributes positively to immunity against necrotrophic fungus *Botrytis cinerea*. *Molecular Plant-Microbe Interactions* **32**:566-582. 10.1094/MPMI-04-18-0097-R.

Livak, K.J., and Schmittgen, T.D. (2001). Analysis of relative gene expression data using real-time quantitative PCR and the $2^{-\Delta\Delta CT}$ method. *Methods* **25**:402-408. 10.1006/meth.2001.1262.

MacLean, A.M., Orlovskis, Z., Kowitwanich, K., Zdziarska, A.M., Angenent, G.C., Immink, R.G.H., and Hogenhout, S.A. (2014). Phytoplasma effector SAP54 hijacks plant reproduction by degrading MADS-box proteins and promotes insect colonization in a RAD23-dependent manner. *Plos Biology* **12**:e1001835. 10.1371/journal.pbio.1001835.

Mejias, J., Bazin, J., Truong, N.M., Chen, Y., Marteu, N., Bouteiller, N., Sawa, S., Crespi, M.D., Vaucheret, H., and Abad, P., et al. (2021). The root-knot nematode

effector MiEFF18 interacts with the plant core spliceosomal protein SmD1 required for giant cell formation. *New Phytologist* **229**:3408-3423. 10.1111/nph.17089.

Mejias, J., Chen, Y., Bazin, J., Truong, N., Mulet, K., Noureddine, Y., Jaubert-Possamai, S., Ranty-Roby, S., Soulé, S., and Abad, P., et al. (2022). Silencing the conserved small nuclear ribonucleoprotein SmD1 target gene alters susceptibility to root-knot nematodes in plants. *Plant Physiology* **189**:1741-1756. 10.1093/plphys/kiac155.

Niu, J., Liu, P., Liu, Q., Chen, C., Guo, Q., Yin, J., Yang, G., and Jian, H. (2016). Msp40 effector of root-knot nematode manipulates plant immunity to facilitate parasitism. *Scientific Reports* **6**:19443. 10.1038/srep19443.

Nomura, K., Debroy, S., Lee, Y.H., Pumplin, N., Jones, J., and He, S.Y. (2006). A bacterial virulence protein suppresses host innate immunity to cause plant disease. *Science* **313**:220-223. 10.1126/science.1129523.

Olmo, R., Cabrera, J., Diaz-Manzano, F.E., Ruiz-Ferrer, V., Barcala, M., Ishida, T., Garcia, A., Andres, M.F., Ruiz-Lara, S., and Verdugo, I., et al. (2020). Root-knot nematodes induce gall formation by recruiting developmental pathways of post-embryonic organogenesis and regeneration to promote transient pluripotency. *New Phytologist* **227**:200-215. 10.1111/nph.16521.

Olmo, R., Cabrera, J., Fenoll, C., and Escobar, C. (2019). A role for *ALF4* during gall and giant cell development in the biotic interaction between Arabidopsis and *Meloidogyne* spp. *Physiologia Plantarum* **165**:17-28. 10.1111/ppl.12734.

Olmo, R., Cabrera, J., Moreno-Risueno, M.A., Fukaki, H., Fenoll, C., and Escobar, C. (2017). Molecular transducers from roots are triggered in Arabidopsis leaves by root-knot nematodes for successful feeding site formation: A conserved post-embryogenic *De novo* organogenesis program? *Frontiers in Plant Science* **8**:875. 10.3389/fpls.2017.00875.

Park, H.C., Kim, M.L., Kang, Y.H., Jeon, J.M., Yoo, J.H., Kim, M.C., Park, C.Y., Jeong, J.C., Moon, B.C., and Lee, J.H., et al. (2004). Pathogen- and NaCl-induced expression of the SCaM-4 promoter is mediated in part by a GT-1 Box that interacts with a GT-1-like transcription factor. *Plant Physiology* **135**:2150-2161. 10.1104/pp.104.041442.

Pieterse, C.M.J., Pierik, R., and Van Wees, S.C.M. (2014). Different shades of JAZ during plant growth and defense. *New Phytologist* **204**:261-264. 10.1111/nph.13029.

Portillo, M., Lindsey, K., Casson, S., García-Casado, G., Solano, R., Fenoll, C., and Escobar, C. (2009). Isolation of RNA from laser-capture-microdissected giant cells at early differentiation stages suitable for differential transcriptome analysis. *Molecular Plant Pathology* **10**:523-535. 10.1111/j.1364-3703.2009.00552.x.

Przybylska, A., and Spychalski, M. (2021). Changes in the expression level of genes encoding transcription factors and cell wall-related proteins during *Meloidogyne arenaria* infection of maize (*Zea mays*). *Molecular Biology Reports* **48**:6779-6786. 10.1007/s11033-021-06677-3.

Qi, F., and Zhang, F. (2020). Cell cycle regulation in the plant response to stress. *Frontiers in Plant Science* **10**:1765. 10.3389/fpls.2019.01765.

Reitz, M.U., Gifford, M.L., and Schäfer, P. (2015). Hormone activities and the cell cycle machinery in immunity-triggered growth inhibition. *Journal of Experimental Botany* **66**:2187-2197. 10.1093/jxb/erv106.

Rich-Griffin, C., Eichmann, R., Reitz, M.U., Hermann, S., Woolley-Allen, K., Brown, P.E., Wiwatdirekkul, K., Esteban, E., Pasha, A., and Kogel, K., et al. (2020). Regulation of cell type-specific immunity networks in Arabidopsis roots. *The Plant Cell* **32**:2742-2762. 10.1105/tpc.20.00154.

Sato, K., Uehara, T., Holbein, J., Sasaki-Sekimoto, Y., Gan, P., Bino, T., Yamaguchi, K., Ichihashi, Y., Maki, N., and Shigenobu, S., et al. (2021). Transcriptomic analysis of resistant and susceptible responses in a new model root-knot nematode infection system using *Solanum torvum* and *Meloidogyne arenaria*. *Frontiers in Plant Science* **12**:680151. 10.3389/fpls.2021.680151.

Schiessl, K., Lilley, J.L.S., Lee, T., Tamvakis, I., Kohlen, W., Bailey, P.C., Thomas, A., Luptak, J., Ramakrishnan, K., and Carpenter, M.D., et al. (2019). *NODULE INCEPTION* recruits the lateral root developmental program for symbiotic nodule organogenesis in *Medicago truncatula*. *Current Biology* **29**:3657-3668. 10.1016/j.cub.2019.09.005.

Schindelin, J., Arganda-Carreras, I., Frise, E., Kaynig, V., Longair, M., Pietzsch, T., Preibisch, S., Rueden, C., Saalfeld, S., and Schmid, B., et al. (2012). Fiji: an open-source platform for biological-image analysis. *Nature Methods* **9**:676-682. 10.1038/nmeth.2019.

Shukla, N., Yadav, R., Kaur, P., Rasmussen, S., Goel, S., Agarwal, M., Jagannath, A., Gupta, R., and Kumar, A. (2018). Transcriptome analysis of root-knot nematode (*Meloidogyne incognita*)-infected tomato (*Solanum lycopersicum*) roots

reveals complex gene expression profiles and metabolic networks of both host and nematode during susceptible and resistance responses. *Molecular Plant Pathology* **19**:615-633. 10.1111/mpp.12547.

Song, H., Lin, B., Huang, Q., Sun, T., Wang, W., Liao, J., and Zhuo, K. (2021). The *Meloidogyne javanica* effector Mj2G02 interferes with jasmonic acid signalling to suppress cell death and promote parasitism in *Arabidopsis*. *Molecular Plant Pathology* **22**:1288-1301. 10.1111/mpp.13111.

Soyano, T., Shimoda, Y., Kawaguchi, M., and Hayashi, M. (2019). A shared gene drives lateral root development and root nodule symbiosis pathways in *Lotus*. *Science* **366**:1021-1023. 10.1126/science.aax2153.

Strader, L., Weijers, D., and Wagner, D. (2022). Plant transcription factors-being in the right place with the right company. *Current Opinion in Plant Biology* **65**:102136. 10.1016/j.pbi.2021.102136.

Suzuki, R., Kanno, Y., Abril-Urias, P., Seo, M., Escobar, C., Tsai, A.Y., and Sawa, S. (2022). Local auxin synthesis mediated by YUCCA4 induced during root-knot nematode infection positively regulates gall growth and nematode development. *Frontiers in Plant Science* **13**:1019427. 10.3389/fpls.2022.1019427.

Suzuki, R., Yamada, M., Higaki, T., Aida, M., Kubo, M., Tsai, A.Y., and Sawa, S. (2021). *PUCHI* regulates giant cell morphology during root-knot nematode infection in *Arabidopsis thaliana*. *Frontiers in Plant Science* **12**:755610. 10.3389/fpls.2021.755610.

Thein, M.C., Winter, A.D., Stepek, G., McCormack, G., Stapleton, G., Johnstone, I.L., and Page, A.P. (2009). Combined extracellular matrix cross-linking activity of the peroxidase MLT-7 and the dual oxidase BLI-3 Is critical for post-embryonic viability in *Caenorhabditis elegans*. *Journal of Biological Chemistry* **284**:17549-17563. 10.1074/jbc.M900831200.

Tian, F., Yang, D., Meng, Y., Jin, J., and Gao, G. (2019). PlantRegMap: charting functional regulatory maps in plants. *Nucleic Acids Research* **48**:D1104-D1113. 10.1093/nar/gkz1020.

Torres-Martínez, H.H., Rodríguez-Alonso, G., Shishkova, S., and Dubrovsky, J.G. (2019). Lateral root primordium morphogenesis in angiosperms. *Frontiers in Plant Science* **10**:206. 10.3389/fpls.2019.00206.

Tudor, J.E., Pallaghy, P.K., Pennington, M.W., and Norton, R.S. (1996). Solution structure of ShK toxin, a novel potassium channel inhibitor from a sea anemone.

Nature Structural Biology **3**:317-320. 10.1038/nsb0496-317.

Üstüner, S., Schäfer, P., and Eichmann, R. (2022). Development specifies, diversifies and empowers root immunity. *EMBO Reports* **23**. 10.15252/embr.202255631.

Waese, J., Fan, J., Pasha, A., Yu, H., Fucile, G., Shi, R., Cumming, M., Kelley, L.A., Sternberg, M.J., and Krishnakumar, V., et al. (2017). ePlant: Visualizing and exploring multiple levels of data for hypothesis generation in plant biology. *The Plant Cell* **29**:1806-1821. 10.1105/tpc.17.00073.

Walter, M., Chaban, C., Schütze, K., Batistic, O., Weckermann, K., Näke, C., Blazevic, D., Grefen, C., Schumacher, K., and Oecking, C., et al. (2004). Visualization of protein interactions in living plant cells using bimolecular fluorescence complementation. *Plant Journal* **40**:428-438. 10.1111/j.1365-313X.2004.02219.x.

Wang, K., He, J., Zhao, Y., Wu, T., Zhou, X., Ding, Y., Kong, L., Wang, X., Wang, Y., and Li, J., et al. (2018). EAR1 Negatively Regulates ABA Signaling by Enhancing 2C Protein Phosphatase Activity. *The Plant Cell* **30**:815-834. 10.1105/tpc.17.00875.

Warmerdam, S., Sterken, M.G., van Schaik, C., Oortwijn, M.E.P., Sukarta, O.C.A., Lozano-Torres, J.L., Dicke, M., Helder, J., Kammenga, J.E., and Goverse, A., et al. (2018). Genome-wide association mapping of the architecture of susceptibility to the root-knot nematode *Meloidogyne incognita* in *Arabidopsis thaliana*. *New Phytologist* **218**:724-737. 10.1111/nph.15034.

Yamaguchi, Y.L., Suzuki, R., Cabrera, J., Nakagami, S., Sagara, T., Ejima, C., Sano, R., Aoki, Y., Olmo, R., and Kurata, T., et al. (2017). Root-knot and cyst nematodes activate procambium-associated genes in *Arabidopsis* roots. *Frontiers in Plant Science* **8**:1195. 10.3389/fpls.2017.01195.

Zhang, L., Davies, L.J., and Elling, A.A. (2015). A *Meloidogyne incognita* effector is imported into the nucleus and exhibits transcriptional activation activity *in planta*. *Molecular Plant Pathology* **16**:48-60. 10.1111/mpp.12160.

Zhang, Q., Zhong, T., E, L., Xu, M., Dai, W., Sun, S., and Ye, J. (2021). GT factor ZmGT-3b is associated with regulation of photosynthesis and defense response to *Fusarium graminearum* infection in maize seedling. *Frontiers in Plant Science* **12**:724133. 10.3389/fpls.2021.724133.

Zhao, J., Li, L., Liu, Q., Liu, P., Li, S., Yang, D., Chen, Y., Pagnotta, S., Favery, B.,

966 **and Abad, P., et al.** (2019). A MIF-like effector suppresses plant immunity and
967 facilitates nematode parasitism by interacting with plant annexins. *Journal of*
968 *Experimental Botany* **70**:5943-5958. 10.1093/jxb/erz348.
969 **Zhao, J., Sun, Q., Quentin, M., Ling, J., Abad, P., Zhang, X., Li, Y., Yang, Y.,**
970 **Favery, B., and Mao, Z., et al.** (2021). A *Meloidogyne incognita* C-type lectin
971 effector targets plant catalases to promote parasitism. *New Phytologist* **232**:2124-
972 2137. 10.1111/nph.17690.
973 **Zhu, Y., Yuan, G., Zhao, R., An, G., Li, W., Si, W., Liu, J., and Sun, D.** (2022).
974 Comparative transcriptome analysis reveals differential gene expression in resistant
975 and susceptible watermelon varieties in response to *Meloidogyne incognita*. *Life*
976 **12**:1003. 10.3390/life12071003.

977

FIGURE LEGENDS

Figure 1. Structure and nuclear localization of *M. incognita* effector Mi2G02. (A) Schematic diagram of the Mi2G02 and mutant Mi2G02 proteins. (B) Subcellular localization of Mi2G02 and mutant Mi2G02 in plant cells. Coding sequences were constructed into *ProSuper*:GFP (C-terminus GFP) vector. Mi2G02 and nuclear localization signal mutants fused with GFP (Mi2G02-GFP, Mi2G02-mu1-GFP, Mi2G02-mu2-GFP and Mi2G02-mu3-GFP) were co-expressed with mcherry in *Nicotiana benthamiana* leaf cells. Empty vectors were used as controls. The fluorescence signal was detected at 48 hours after infiltration. Mi2G02-GFP localized to the nucleus. Mi2G02-mu1-GFP, Mi2G02-mu2-GFP and Mi2G02-mu3-GFP primarily localized to the plasma membrane and cytoplasm. Images were captured by confocal microscopy (Zeiss LSM 700, Germany). GFP, green fluorescent protein. Scale bars, 20 μm. (C) The relative abundance of Mi2G02-GFP or Mi2G02-mu-GFP in cytoplasmic and nuclear fractions was detected using anti-GFP antibodies after transiently expressing in *N. benthamiana* leaf cells. Actin was used as an internal reference for the presence of cytoplasmic proteins and Histone H3 was used as an internal reference for the presence of nuclear proteins.

Figure 2. Host-derived RNA interference (RNAi) and ectopic expression of *Mi2G02* in *A. thaliana* alter plants susceptibility to *M. incognita* and root development. (A) *Mi2G02* expression level in three homozygous RNAi lines (Mi2G02-Ri-1, Mi2G02-Ri-2 and Mi2G02-Ri-4), gfp-RNAi line (GFP-Ri) and wild type (WT) were determined at 10 days post infection (dpi) of *M. incognita* by RT-qPCR. *GAPDH* was used as an internal control. The values shown are means ± SE (n = 3). Different letters indicate significant differences (P<0.05, one-way ANOVA). (B) Gall numbers and egg mass numbers per plant at 35 dpi. Values are presented as means ± SD (n=18). Different letters indicate significant differences (P<0.05, one-way ANOVA). See also Figure S1B. (C) Giant cell areas of *M. incognita*-induced galls in the *A. thaliana* Mi2G02-Ri lines were significantly reduced. Gall sections at 14 days post infection (dpi) were stained with toluidine-blue. Relatively smaller giant cells were observed in Mi2G02-Ri mature galls at 14 dpi compared with the WT and GFP-Ri controls. Data are the average surface areas ± SD (n=10) for each line. Different letters indicate significant differences (P<0.05, one-way ANOVA). Asterisk, giant cell; N, nematode. Bars, 100 μm. (D) *A. thaliana* phenotypes and relative root length of

Mi2G02 ectopic expressing *A. thaliana* lines compared with wild-type. Data represents the average length ± SD (n=10). Different letters indicate significant differences (P<0.05, one-way ANOVA). Scale bar, 1 cm. See also Figure S2C. (E) Expression of *Mi2G02* in *A. thaliana* increased susceptibility to *M. incognita*. Two independent Mi2G02-T3 lines were inoculated with *M. incognita* pre-J2s. Total numbers of galls and egg masses were counted at 35 dpi. *M. incognita* inoculated wild-type *A. thaliana* plant was used as control. Data are the average numbers per plant ± SD (n=16). Different letters indicate significant differences (P<0.05, one-way ANOVA). See also Figure S2D.

Figure 3. The Mi2G02 effector interacts with GT-3a in the nuclei. (A) Schematic representation of the intact and truncated Mi2G02 (with or without ShKT domain) and GT-3a (with or without DNA binding domain) used for yeast two-hybrid assays (Y2Hs). (B) Pairwise Y2H tests were performed to investigate the interactions between Mi2G02 or ShKT domains and GT-3a or DNA binding (DB) domain. Left column, yeast cell growth carrying the baits in pGBKT7 vector (BD) and preys in pGADT7 (AD) grown on SD/-Trp-Leu (SD-WL) medium indicating successful transformation of the yeast with both plasmids; right column, yeast cell growth on the selective dropout medium (SD/-Trp-Leu-His, SD-WLH) following the addition of 20 mg/ml X-α-gal indicating protein interaction. Yeast cells containing p53 and SV40 large T-antigen were used as positive control, and yeast cells containing Lamin and SV40 large T-antigen were used as negative control. (C) Pairwise Y2H tests were performed to investigate the interactions between Mi2G02 mutants and GT-3a. (D) Mi2G02 colocalizes with GT-3a in *N. benthamiana* cell nuclei. Mi2G02 fused with GFP in C-terminus (Mi2G02-GFP) and GT-3a fused with mcherry in N-terminus (mcherry-GT-3a) were co-expressed in *N. benthamiana* leaf cells. The fluorescence signal was detected at 48 h after infiltration. Images were captured by confocal microscopy. Scale bars, 20 μm. (E) Bimolecular fluorescence complementation (BiFC) experiments demonstrate the interaction between Mi2G02 and GT-3a. *N. benthamiana* leaves were transformed with different combinations of nEYFP and cEYFP fused vectors. Images were obtained 48 h after co-expression. Yellow fluorescent protein (YFP) fluorescence signals were observed in the nuclei in leaves co-infiltrated with nEYFP-Mi2G02 and GT-3a-cEYFP. Scale bars, 20 μm. See also Figure S3C. (F) Determination of the interaction between Mi2G02 and GT-3a

through luciferase complementation assay (LCA). *A. tumefaciens* harboring different combinations of plasmids were infiltrated into indicated regions of *N. benthamiana* leaves. The luciferase activities were recorded at 2 days post agro-infiltration by spraying 1 mM luciferin solution onto the infiltrated leaves, and the luciferase activity was detected with a low-light cooled CCD imaging apparatus. Luciferase activity was depicted with false color from low (black) to high (white). The protein levels of Mi2G02-NLuc, Mi2G02-mu1-NLuc, Mi2G02-mu2-NLuc, Mi2G02-mu3-NLuc, CLuc-GT-3a, GUS-NLuc, CLuc-GUS were determined by western blotting using anti-Luciferase antibody. Ponceau S (P) staining provided a loading control. (G) Mi2G02 associates with GT-3a in a co-immunoprecipitation (Co-IP) assay. *A. tumefaciens* harboring different combinations of plasmids were infiltrated into *N. benthamiana* leaves. Co-IP was performed with BeyoMag™ Anti HA Magnetic Beads, and the eluted protein was detected using western blotting with antibody against HA and GFP. GFP, green fluorescent protein. P, ponceau staining indicates samples loading.

Figure 4. GT-3a is involved in *M. incognita* parasitism and lateral roots development. (A) The activity of *GT-3a* promoter was analysed in uninfected roots and in galls induced by *M. incognita* in *A. thaliana* expressing the *ProGT-3a:GUS* construct. Scale bars, 100 μm. dpi, days-post infection. (B) *A. thaliana* phenotypes, relative root length and relative lateral root numbers of *Mi2G02* ectopic expressing *A. thaliana* lines compared with wild-type. Data represents the average length ± SD (n=10) and the average number ± SD (n=10). Different letters indicate significant differences (P<0.05, one-way ANOVA). Scale bar, 1 cm. See also Figure S4H. (C) Lateral root density calculated as the number of emerged lateral roots divided by total primary root length. Different letters indicate significant differences (P<0.05, one-way ANOVA). (D) Overexpression of *GT-3a* in *A. thaliana* increased susceptibility to *M. incognita*. Two independent *GT-3a* ectopic expressing T3 lines were inoculated with *M. incognita* pre-J2s. Total numbers of galls and egg masses were counted at 35 dpi. *M. incognita* inoculated wild-type *A. thaliana* plant was used as control. Data are the average number ± SD (n=18). Different letters indicate significant differences (P<0.05, one-way ANOVA). See also Figure S5A. (E) The *gt-3a* T-DNA knockout mutants (SALK_134703 and SALK_040448) were less susceptible to *M. incognita* compared with the wild-type, as indicated by the mean

numbers of galls and egg masses. Data are the average number ± SD (n=26). Different letters indicate significant differences (*P*<0.05, one-way ANOVA). See also Figure S5B. (F) Giant cell areas of *M. incognita*-induced galls in the *A. thaliana gt-3a* T-DNA knockout mutant lines were significantly reduced. Gall sections at 21 dpi were stained with toluidine-blue. Relatively smaller giant cells were observed in *gt-3a* T-DNA knockout mutant lines compared with the wild-type. Data are the average surface area ± SD (n=10). Different letters indicate significant differences (*P*<0.05, one-way ANOVA). Asterisk, giant cell; N, nematode. Bars, 100 μm.

Figure 5. Targeting and suppression of *TOZ* and *RAD23C* by GT-3a and the susceptibility of *toz* and *rad23c* knockout mutant lines to *M. incognita*. (A) Transcriptional activity of GT-3a in yeast cells. The yeast AH109 strain expressing pCL-1, GT-3a, GT-3a with or without DNA binding domain (GT-3a-DB or GT-3a-ΔDB) grew on Yeast Peptone Dextrose Adenine Agar (YPDA) or the selective medium SD-His-Trp with or without X-α-gal. The pCL-1 encoding the full-length GAL4 and the empty vector pGBKT7 (BD) were used as positive and negative controls, respectively. (B) Yeast one-hybrid (Y1H) experiments showed GT-3a bound to the promoter of *TOZ*, *RAD23C* and *WRKY2*. Promoter fragments containing -GTTAC- or -CACGTG- element were cloned into pLacZi vector, GT-3a was cloned into pB42AD vector, and then pLacZi vector co-transformed with pB42AD-GT-3a into yeast strain EGY48. The yeast transformants were spotted on the plate SD/-Ura-Trp with or without 20 mg/ml X-gal. pB42AD-p53 and pLacZi-p53 were used as a positive control. (C) Luciferase reporter assays of GT-3a-induced suppression of *TOZ* and *RAD23C* expression in *N. benthamiana*. LUC activity was measured by normalizing to REN signal. Values are means ± SE (n = 4). Asterisks mark significant differences according to two-tailed Student's *t* test, ****P*<0.001. Similar results were obtained from three independent experiments (biological replicates). (D) qRT-PCR analysis of *TOZ* and *RAD23C* expression in wild type *A. thaliana* and *GT-3a* overexpressing *A. thaliana* lines. *UBP22* (*AT5G10790*) was used as an internal control. Data represent the mean of three independent experiments ± SE (n=3). Similar results were obtained from three independent experiments (biological replicates). Different letters indicate significant differences (*P*<0.05, one-way ANOVA). (E) EMSA assays confirmed GT-3a-His could direct bind to the promoter of *TOZ* and *RAD23C*. Promoter fragments containing -GTTAC- element (P1 probe) or -

CACGTG- element (P2 probe) or mutant elements (-AAAAA- or -AAAAAA-) were labeled with biotin as probes. 6×His alone served as a negative control. Unlabeled probes were used as competing probes.

Figure 6. Mi2G02 stabilizes GT-3a to promote its function in suppression of *TOZ* and *RAD23C* expression for nematode parasitism. (A) The *rad23c* T-DNA knockout mutant is more susceptible than the wild type to *M. incognita*. The *rad23c* KO mutant (*SALK_068091*) was inoculated with nematodes, and the numbers of galls and egg masses were counted 35 days post-inoculation. The data presented are the mean numbers per plant ± SD (*n*=28). Similar results were obtained in three independent experiments. Asterisks indicate differences that were significant in two-tailed Student's *t* tests, ***P*<0.01. See also Figure S7E. (B) Luciferase reporter assays showed that the GT-3a-induced suppression of *TOZ* and *RAD23C* expression in *N. benthamiana* was enhanced by Mi2G02 expression. LUC activity was determined and normalized against the REN signal. The data presented are the means of three independent experiments ± SEM (*n*=4). Different letters indicate significant differences (*P*<0.05, one-way ANOVA). (C) Mi2G02 stabilizes the GT-3a-GFP fluorescence intensity. *GT-3a* was co-expressed with *Mi2G02* in *N. benthamiana* leaves, and Mi2G02 mutants and MiEFF18 (a nuclear *M. incognita* effector not interacted with GT-3a) were used as controls. The GT-3a-GFP fluorescence was detected with confocal microscopy (LSM700, Zeiss) 48 h after infiltration. Graphs showed the fluorescence intensity profiles across the arrows in the GFP images. Bar = 10 μm. See also Figure S8. (D) Mi2G02 stabilizes the GT-3a protein, leading to its accumulation. *GT-3a* was co-expressed with *Mi2G02* or *GFP* in *N. benthamiana* leaves. The GT-3a protein was detected with an anti-GFP antibody. Band intensity was determined with ImageJ software and is indicated below the bands. CBB, Coomassie brilliant blue staining, and P, Ponceau staining, were used to check protein sample loading. (E) Mi2G02 inhibits of the GT-3a degradation via 26S proteasome pathway *in vivo*. GT-3a-GFP was co-expressed with Mi2G02-HA and Mi2G02 mutants in *N. benthamiana* leaves, respectively. The 26S proteasome inhibitor MG132 (100 μM) was infiltrated into *N. benthamiana* leaves 24 h before protein extraction. Band intensity was determined by ImageJ software and is indicated below the bands.

Figure 7 A proposed working model illustrating the molecular mechanism of the interaction among Mi2G02, GT-3a and *TOZ*, *RAD23C* in the nematode parasitism. In the early stage of *M. incognita* parasitism, Mi2G02 effector protein is secreted into the plant cell and translocates to the plant nucleus, where targets the transcription factor GT-3a and stabilizes its proteins level by inhibiting 26S proteasome pathway, leading to the suppression of *TOZ* and *RAD23C* expression for nematode feeding cells formation and development.

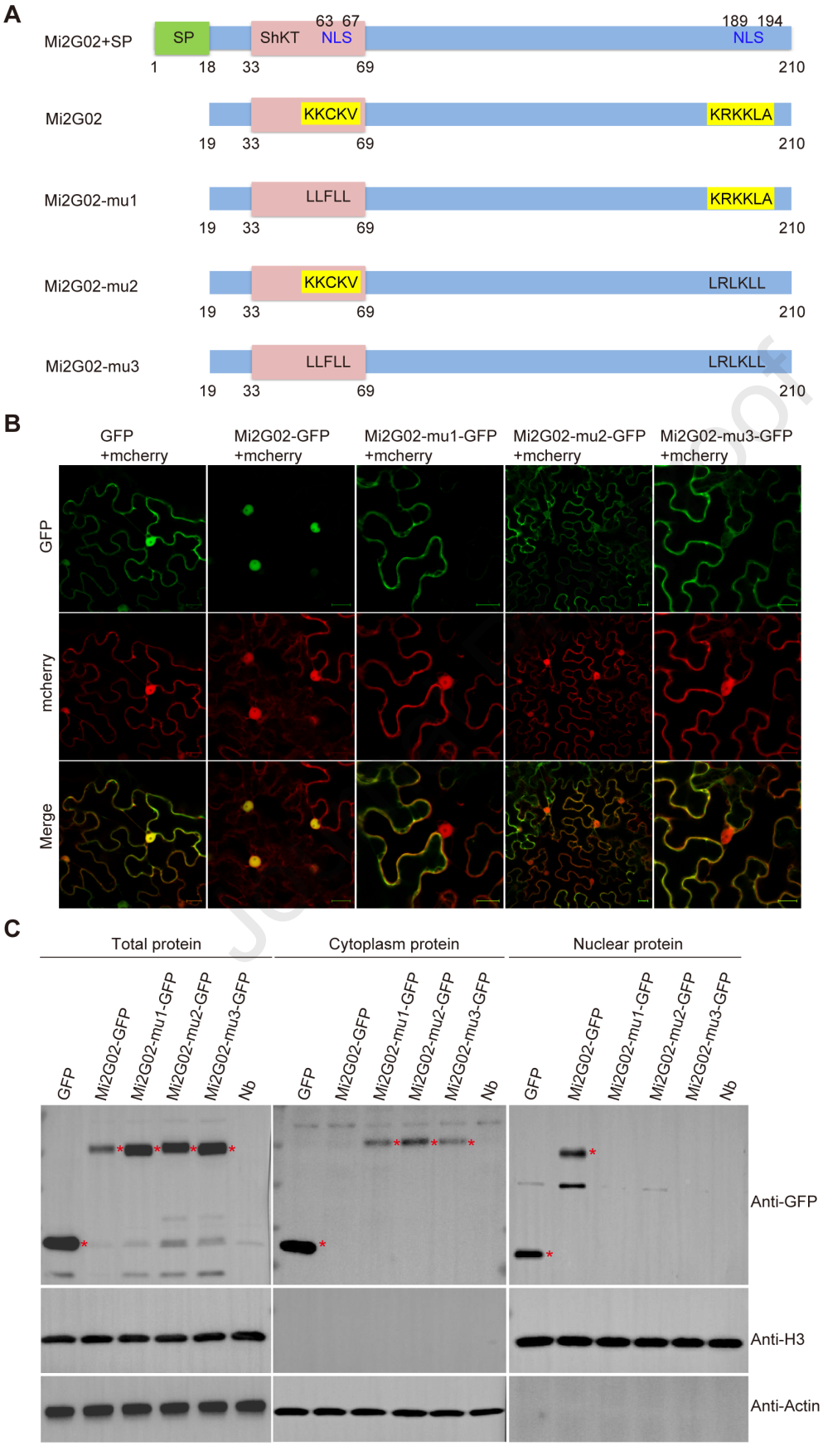
A
Mi2G02+SP
SP
ShKT
63 67
NLS
189 194
NLS
1 18 33 69 210
Mi2G02
KKCKV
KRKKLA
19 33 69 210
Mi2G02-mu1
LLFLL
KRKKLA
19 33 69 210
Mi2G02-mu2
KKCKV
LRLKLL
19 33 69 210
Mi2G02-mu3
LLFLL
LRLKLL
19 33 69 210
B
GFP +mcherry
Mi2G02-GFP +mcherry
Mi2G02-mu1-GFP +mcherry
Mi2G02-mu2-GFP +mcherry
Mi2G02-mu3-GFP +mcherry
GFP
mcherry
Merge
C
Total protein
Cytoplasm protein
Nuclear protein
GFP
Mi2G02-GFP
Mi2G02-mu1-GFP
Mi2G02-mu2-GFP
Mi2G02-mu3-GFP
Nb
Anti-GFP
Anti-H3
Anti-Actin

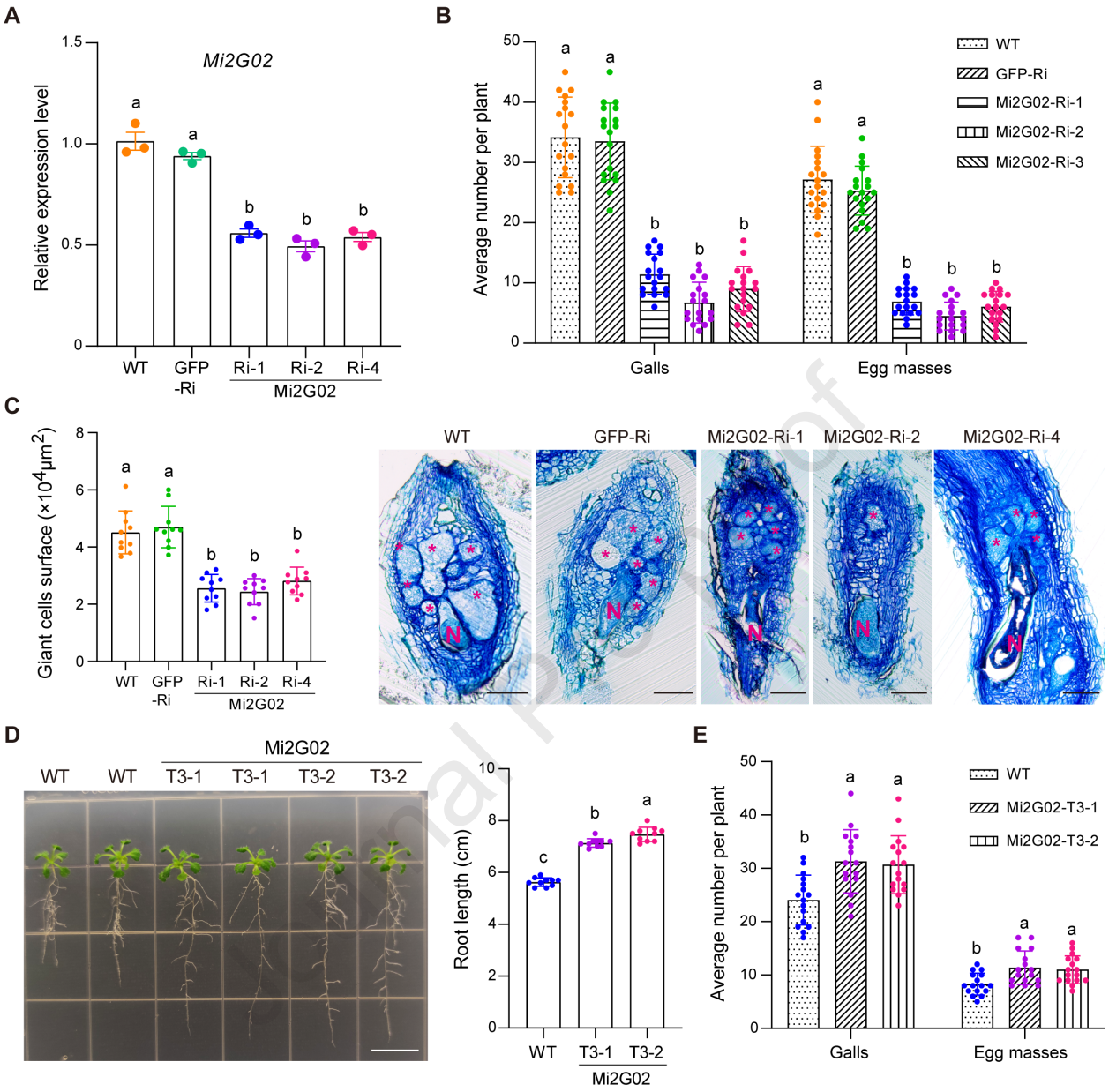
A
Mi2G02
Relative expression level
1.5
1.0
0.5
0
a
a
b
b
b
WT
GFP -Ri
Ri-1
Ri-2
Ri-4
Mi2G02
B
Average number per plant
50
40
30
20
10
0
WT
GFP-Ri
Mi2G02-Ri-1
Mi2G02-Ri-2
Mi2G02-Ri-3
Galls
Egg masses
C
Giant cells surface (×10^4μm^2)
8
6
4
2
0
WT
GFP -Ri
Ri-1
Ri-2
Ri-4
Mi2G02
WT
GFP-Ri
Mi2G02-Ri-1
Mi2G02-Ri-2
Mi2G02-Ri-4
N
D
Mi2G02
WT
WT
T3-1
T3-1
T3-2
T3-2
Root length (cm)
10
8
6
4
2
0
c
b
a
WT
T3-1
T3-2
Mi2G02
E
Average number per plant
50
40
30
20
10
0
WT
Mi2G02-T3-1
Mi2G02-T3-2
Galls
Egg masses

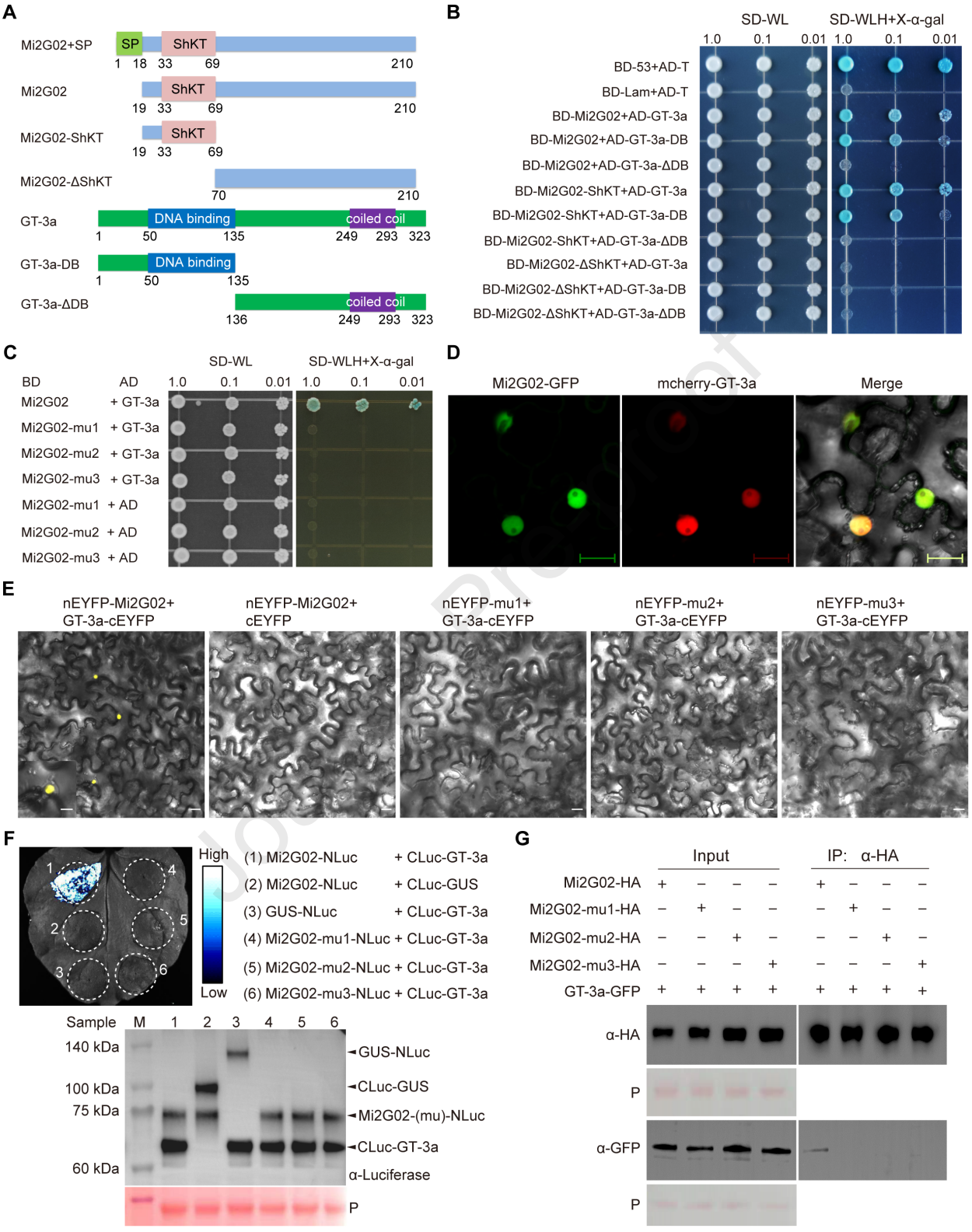
A
Mi2G02+SP
SP
ShKT
1 18 33 69 210
Mi2G02
ShKT
19 33 69 210
Mi2G02-ShKT
ShKT
19 33 69
Mi2G02-ΔShKT
70 210
GT-3a
DNA binding
coiled coil
1 50 135 249 293 323
GT-3a-DB
DNA binding
1 50 135
GT-3a-ΔDB
coiled coil
136 249 293 323
B
SD-WL
SD-WLH+X-α-gal
1.0 0.1 0.01 1.0 0.1 0.01
BD-53+AD-T
BD-Lam+AD-T
BD-Mi2G02+AD-GT-3a
BD-Mi2G02+AD-GT-3a-DB
BD-Mi2G02+AD-GT-3a-ΔDB
BD-Mi2G02-ShKT+AD-GT-3a
BD-Mi2G02-ShKT+AD-GT-3a-DB
BD-Mi2G02-ShKT+AD-GT-3a-ΔDB
BD-Mi2G02-ΔShKT+AD-GT-3a
BD-Mi2G02-ΔShKT+AD-GT-3a-DB
BD-Mi2G02-ΔShKT+AD-GT-3a-ΔDB
C
SD-WL
SD-WLH+X-α-gal
BD AD 1.0 0.1 0.01 1.0 0.1 0.01
Mi2G02 + GT-3a
Mi2G02-mu1 + GT-3a
Mi2G02-mu2 + GT-3a
Mi2G02-mu3 + GT-3a
Mi2G02-mu1 + AD
Mi2G02-mu2 + AD
Mi2G02-mu3 + AD
D
Mi2G02-GFP
mcherry-GT-3a
Merge
E
nEYFP-Mi2G02+ GT-3a-cEYFP
nEYFP-Mi2G02+ cEYFP
nEYFP-mu1+ GT-3a-cEYFP
nEYFP-mu2+ GT-3a-cEYFP
nEYFP-mu3+ GT-3a-cEYFP
F
1
2
3
4
5
6
High
Low
(1) Mi2G02-NLuc + CLuc-GT-3a
(2) Mi2G02-NLuc + CLuc-GUS
(3) GUS-NLuc + CLuc-GT-3a
(4) Mi2G02-mu1-NLuc + CLuc-GT-3a
(5) Mi2G02-mu2-NLuc + CLuc-GT-3a
(6) Mi2G02-mu3-NLuc + CLuc-GT-3a
Sample M 1 2 3 4 5 6
140 kDa
100 kDa
75 kDa
60 kDa
GUS-NLuc
CLuc-GUS
Mi2G02-(mu)-NLuc
CLuc-GT-3a
α-Luciferase
P
G
Input
IP: α-HA
Mi2G02-HA + – – – + – – –
Mi2G02-mu1-HA – + – – – + – –
Mi2G02-mu2-HA – – + – – – + –
Mi2G02-mu3-HA – – – + – – – +
GT-3a-GFP + + + + + + + +
α-HA
P
α-GFP
P

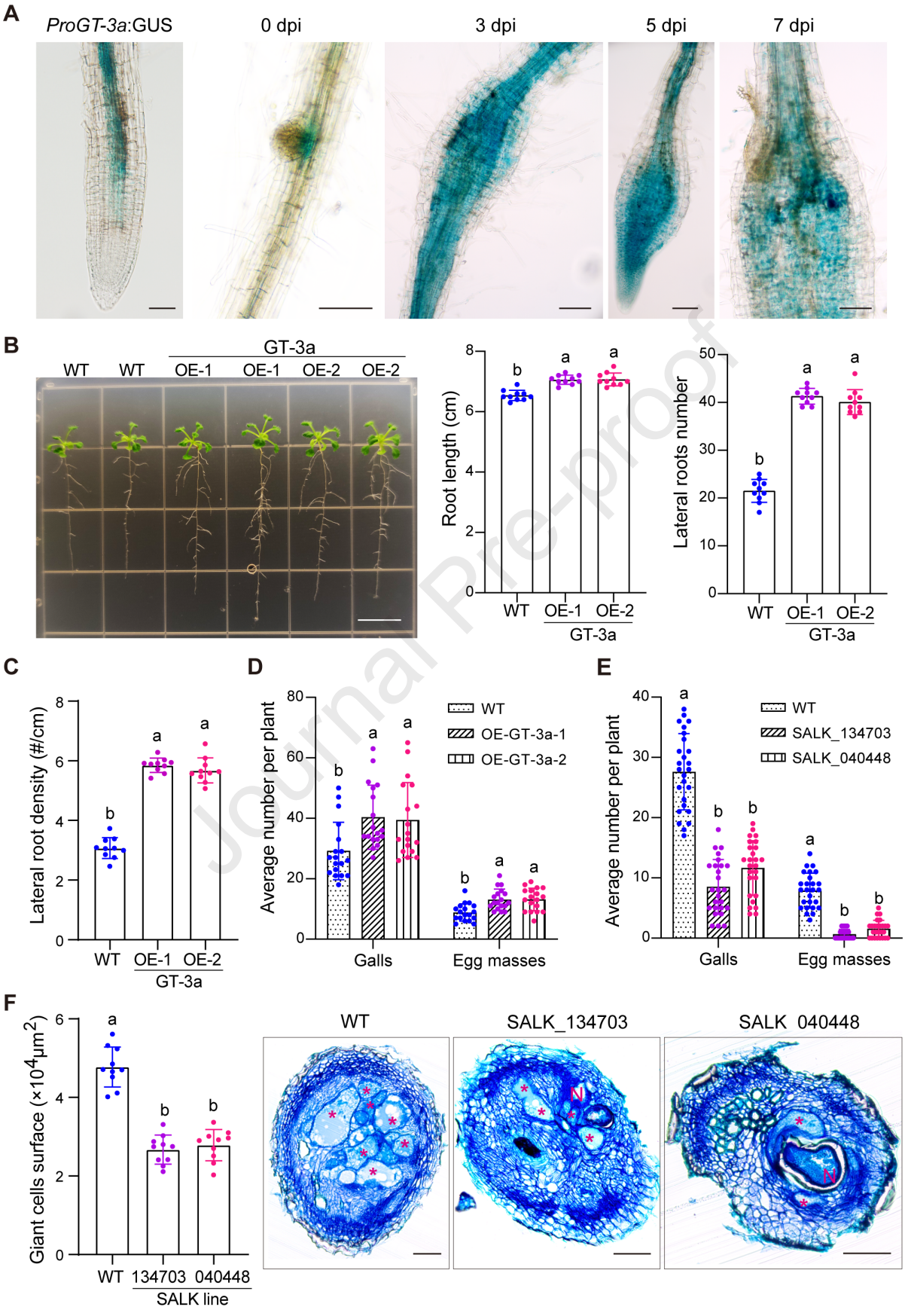

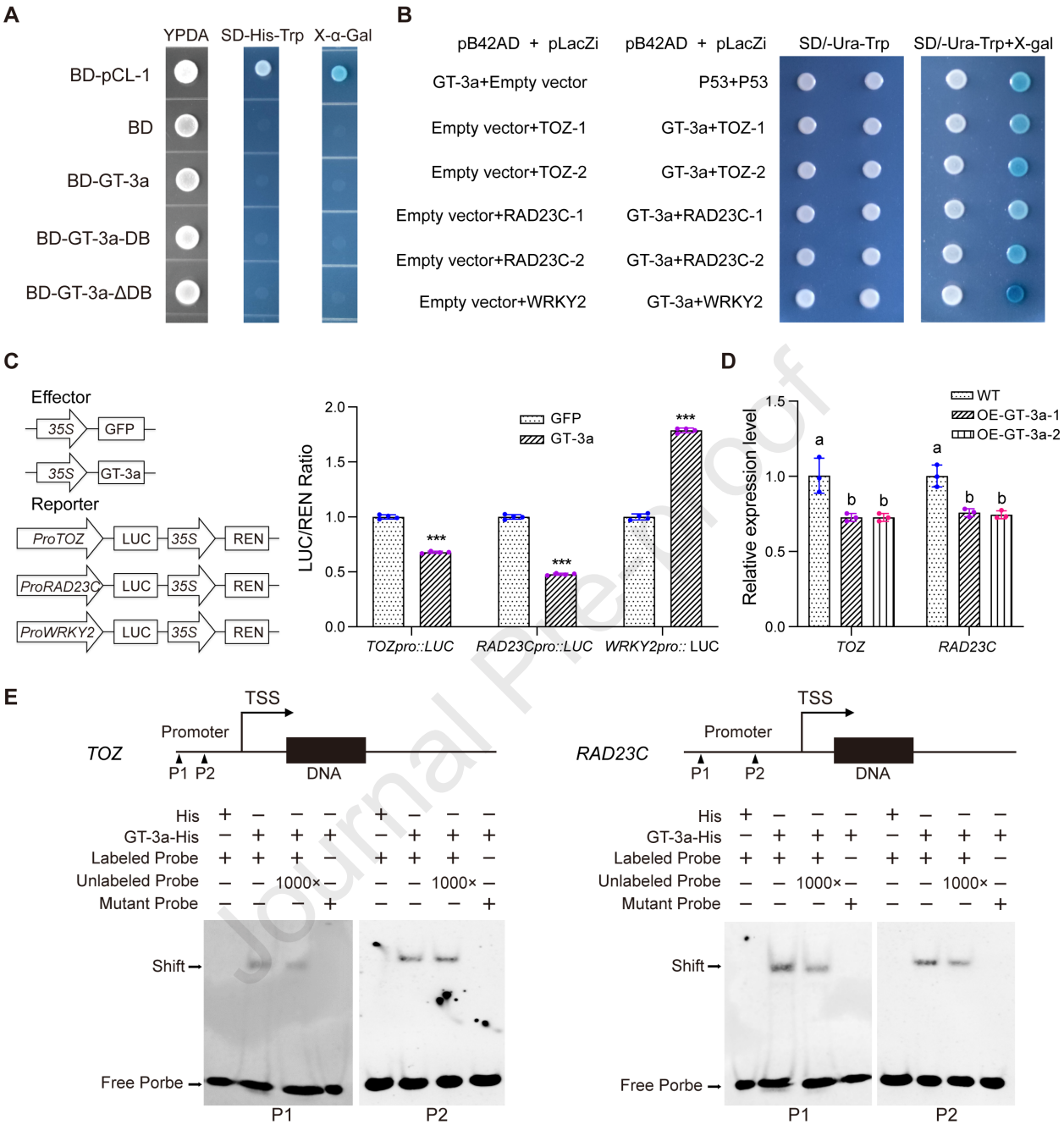

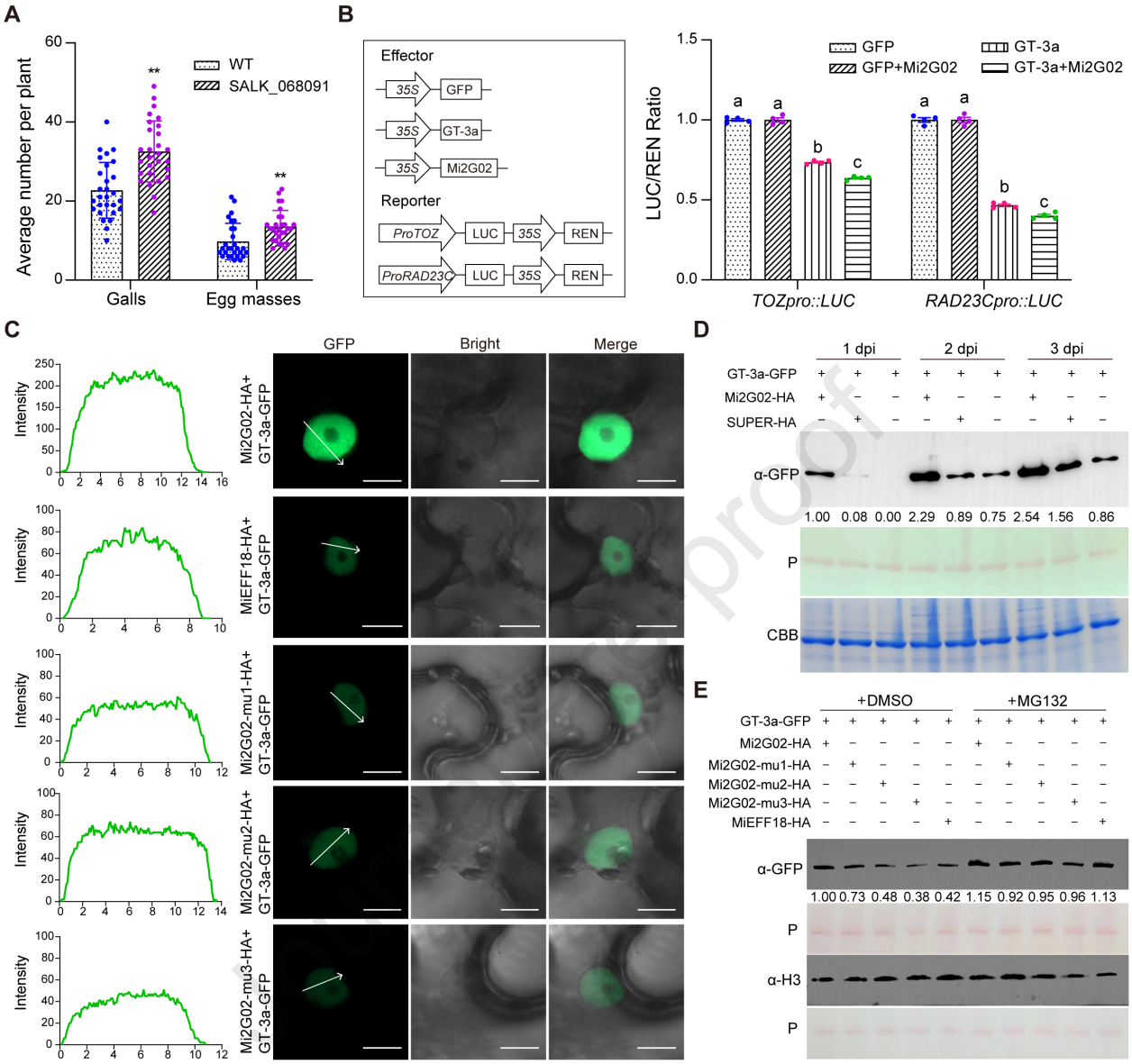
A
Average number per plant
WT
SALK_068091
Galls
Egg masses
B
Effector
35S
GFP
GT-3a
Mi2G02
Reporter
ProTOZ
ProRAD23C
LUC
REN
GFP
GFP+Mi2G02
GT-3a
GT-3a+Mi2G02
LUC/REN Ratio
TOZpro::LUC
RAD23Cpro::LUC
C
GFP
Bright
Merge
Intensity
Mi2G02-HA+ GT-3a-GFP
MiEFF18-HA+ GT-3a-GFP
Mi2G02-mu1-HA+ GT-3a-GFP
Mi2G02-mu2-HA+ GT-3a-GFP
Mi2G02-mu3-HA+ GT-3a-GFP
D
1 dpi
2 dpi
3 dpi
GT-3a-GFP
Mi2G02-HA
SUPER-HA
α-GFP
1.00 0.08 0.00 2.29 0.89 0.75 2.54 1.56 0.86
P
CBB
E
+DMSO
+MG132
GT-3a-GFP
Mi2G02-HA
Mi2G02-mu1-HA
Mi2G02-mu2-HA
Mi2G02-mu3-HA
MiEFF18-HA
α-GFP
1.00 0.73 0.48 0.38 0.42 1.15 0.92 0.95 0.96 1.13
P
α-H3
P